Cellular/Molecular

Subregion-Specific Regulation of Dopamine D1 Receptor Signaling in the Striatum: Implication for L-DOPA-Induced Dyskinesia

Keita Sugiyama,[1] Mahomi Kuroiwa,[1] Takahide Shuto,[1] Yoshinori N. Ohnishi,[1] Yukie Kawahara,[1] Yuta Miyamoto,[2] Takaichi Fukuda,[2] and Akinori Nishi[1]

[1]Department of Pharmacology, Kurume University School of Medicine, Kurume, Fukuoka 830-0011, Japan, and [2]Department of Anatomy and Neurobiology, Graduate School of Medical Sciences, Kumamoto University, Kumamoto, Kumamoto 860-8556, Japan

The striatum is the main structure of the basal ganglia. The striatum receives inputs from various cortical areas, and its subregions play distinct roles in motor and emotional functions. Recently, striatal maps based on corticostriatal connectivity and striosome-matrix compartmentalization were developed, and we were able to subdivide the striatum into seven subregions. Dopaminergic modulation of the excitability of medium spiny neurons (MSNs) is critical for striatal function. In this study, we investigated the functional properties of dopamine signaling in seven subregions of the striatum from male mice. By monitoring the phosphorylation of PKA substrates including DARPP-32 in mouse striatal slices, we identified two subregions with low D1 receptor signaling: the dorsolateral portion of the intermediate/rostral part (DL-IR) and the intermediate/caudal part (IC). Low D1 receptor signaling in the two subregions was maintained by phosphodiesterase (PDE)10A and muscarinic M4 receptors. In an animal model of 6-hydroxydopamine (6-OHDA)-induced hemi-parkinsonism, D1 receptor signaling was upregulated in almost all subregions including the DL-IR, but not in the IC. When L-DOPA-induced dyskinesia (LID) was developed, D1 receptor signaling in the IC was upregulated and correlated with the severity of LID. Our results suggest that the function of the striatum is maintained through the subregion-specific regulation of dopamine D1 receptor signaling and that the aberrant activation of D1 receptor signaling in the IC is involved in LID. Future studies focusing on D1 receptor signaling in the IC of the striatum will facilitate the development of novel therapeutics for LID.

Key words: **D1 receptor; DARPP-32; dopamine; L-DOPA-induced dyskinesia; striatum**

Significance Statement

Recent progress in striatal mapping based on corticostriatal connectivity and striosome-matrix compartmentalization allowed us to subdivide the striatum into seven subregions. Analyses of D1 receptor signaling in the seven subregions identified two unique subregions with low D1 receptor signaling: the dorsolateral portion of the intermediate/rostral part (DL-IR) and the intermediate/caudal part (IC). Aberrant activation of D1 receptor signaling in the IC is involved in L-DOPA-induced dyskinesia (LID). Previous studies of LID have mainly focused on the DL-IR, but not on the IC of the striatum. Future studies to clarify aberrant D1 receptor signaling in the IC are required to develop novel therapeutics for LID.

Introduction

The striatum is the main structure of the basal ganglia, and the function of two types of striatal projection neurons, the D1-type/direct pathway and D2-type/indirect pathway medium spiny neurons (MSNs), is largely regulated by excitatory glutamatergic inputs from the cortex and thalamus, modulatory dopaminergic inputs from the substantia nigra pars compacta (SNpc) and ventral tegmental area (VTA), and modulatory tone of cholinergic interneurons. The striatum is roughly divided into three subregions based on the topographical organization of corticostriatal projections: the dorsolateral striatum projected from the sensorimotor cortex, the dorsomedial striatum projected from the associative cortex, and the ventral striatum or the nucleus accumbens (NAc) projected from the limbic cortex (Alexander and Crutcher, 1990; Voorn et al., 2004; Yin and Knowlton, 2006). Recent comprehensive projectome analyses have developed a detailed map of corticostriatal connectivity (Hintiryan et al., 2016; Hunnicutt et al., 2016). Hintiryan et al. (2016) subdivided

Received Feb. 17, 2021; revised June 2, 2021; accepted June 7, 2021.

Author contributions: K.S., Y.N.O., Y.K., Y.M., T.F., and A.N. designed research; K.S., M.K., and T.S. performed research; K.S., Y.N.O., Y.K., and A.N. analyzed data; K.S. and A.N. wrote the paper.

This work was supported by Scientific Research from the Japan Society for the Promotion of Science Grants-in-Aid 16H05135 and 19H03410 (to A.N.) and 16K10198 (to M.K.).

The authors declare no competing financial interests.

Correspondence should be addressed to Akinori Nishi at nishia@med.kurume-u.ac.jp.

https://doi.org/10.1523/JNEUROSCI.0373-21.2021

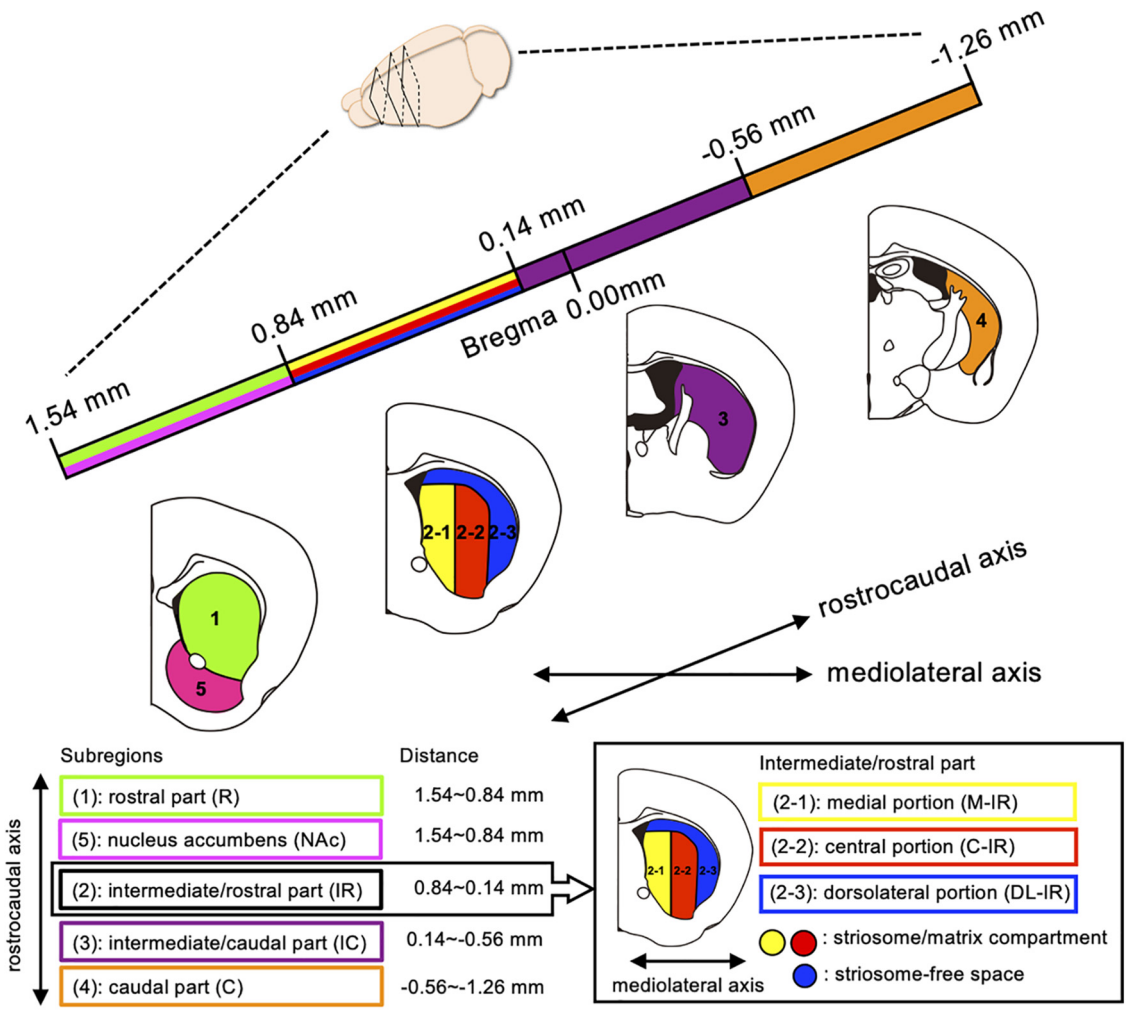

Figure 1. Preparation of coronal slices from the seven subregions of the striatum. Coronal brain slices were prepared from four rostrocaudal levels (starting 1.54 mm anterior to bregma and continuing posterior in 700-μm steps). Striatal slices of six subregions along the rostrocaudal axis (1)–(4) and the mediolateral axis (2-1)–(2-3) were collected from the dorsal striatum, and striatal slices of subregion (5) were collected from the ventral striatum [nucleus accumbens (NAc)]. The position along the rostrocaudal axis is shown as the distance from the bregma level. The intermediate part is divided into the rostral [(2-1), (2-2), and (2-3)] and caudal (3) parts at the level of the anterior commissure crossing the midline (0.14 mm anterior to the bregma). Subregions (2-1) and (2-2) and subregion (2-3) correspond to the striosome-rich regions and the striosome-free space, respectively (Miyamoto et al., 2018).

the large undivided structure of the striatum into 29 subregions based on corticostriatal connectivity, which are located in the rostral, intermediate, and caudal parts of the striatum along the rostrocaudal axis. Each striatal subregion connected to a specific cortical area has distinct functions and synaptic plasticity (Hintiryan et al., 2016; Hunnicutt et al., 2016).

With another anatomic view for classification, the striatum is subdivided into two compartments called the striosomes, also known as patches, and the matrix (Graybiel et al., 1981; Herkenham and Pert, 1981; Gerfen, 1984). Studies of cortical projections have shown that the striosomes predominantly receive cortical inputs from the limbic regions, whereas the matrix mainly receives cortical inputs from the associative and sensorimotor regions (Crittenden and Graybiel, 2011). Miyamoto et al. (2018) reported a striosome-based map of the mouse striatum, in which intrastriatal domains were occupied with five types of striosomes, discriminated with diverse immunoreactivity for the μ-opioid receptor, substance P and enkephalin, and the striosome-free space. The internal structure-based map of the striatum was correlated with the corticostriatal connectivity and distribution patterns of D1-type and D2-type MSNs. The striosome-free space is located in the dorsolateral region of the striatum and receives inputs preferentially from the sensorimotor cortex.

Dopamine plays a central role in the regulation of psychomotor function (Bromberg-Martin et al., 2010; Gerfen and Surmeier, 2011). The effect of dopamine is largely mediated through the regulation of the cAMP/PKA signaling cascade. In the striatum, the expression of dopamine D1 and D2 receptors is segregated into D1-type and D2-type MSNs, respectively (Hersch et al., 1995; Bertran-Gonzalez et al., 2010). Dopamine acting on D1 receptors activates cAMP/PKA signaling, leading to the phosphorylation of PKA-dependent substrates such as dopamine-regulated and cAMP-regulated phosphoprotein of M_r 32 kDa (DARPP-32), AMPA receptor GluA1 subunit, and extracellular receptor kinase (ERK) in D1-type MSNs (Greengard et al., 1999; Svenningsson et al., 2004), whereas dopamine acting on D2 receptors inhibits cAMP/PKA signaling in D2-type MSNs. Phosphorylation of DARPP-32 at Thr34 by PKA converts DARPP-32 into a potent inhibitor of protein phosphatase-1, thereby controlling the phosphorylation state and activity of downstream targets including GluA1 and ERK (Greengard et al., 1999;

Table 1. Statistical analysis for Figure 2

Set of data	Type of statistical analysis	Results of statistical analysis	
A, P-Thr34 D32/D32			
The basal phosphorylation levels	One-way ANOVA	$F_{(6,65)} = 2.005$	$p = 0.0776$
SKF81297 effect in each subregion			
Subregion (1): control vs SKF	Paired *t* test	$t_{(10)} = 3.967$	$p = 0.0027$
Subregion (2-1): control vs SKF	*t* test (Welch's-correction)	$t_{(10.18)} = 4.245$	$p = 0.0016$
Subregion (2-2): control vs SKF	*t* test (Welch's-correction)	$t_{(10.69)} = 4.092$	$p = 0.0019$
Subregion (2-3): control vs SKF	*t* test (Welch's-correction)	$t_{(13.81)} = 4.864$	$p < 0.001$
Subregion (3): control vs SKF	*t* test (Welch's-correction)	$t_{(11.72)} = 1.772$	$p = 0.1023$
Subregion (4): control vs SKF	*t* test (Welch's-correction)	$t_{(12.94)} = 2.999$	$p = 0.0103$
Subregion (5): control vs SKF	*t* test (Welch's-correction)	$t_{(5.11)} = 2.614$	$p = 0.0465$
Two-way ANOVA for mediolateral axis			
SKF effect	Two-way ANOVA	$F_{(1,60)} = 48.91$	$p < 0.001$
Subregion effect	Two-way ANOVA	$F_{(2,60)} = 1.577$	$p = 0.2151$
SKF-subregion interaction	Two-way ANOVA	$F_{(2,60)} = 2.644$	$p = 0.0794$
SKF: subregion (2-1) vs (2-2)	Bonferroni *post hoc* test		$p = 0.5884$
SKF: subregion (2-1) vs (2-3)	Bonferroni *post hoc* test		$p = 0.0168$
SKF: subregion (2-2) vs (2-3)	Bonferroni *post hoc* test		$p = 0.3674$
B, P-Ser845 GluA1/GluA1			
The basal phosphorylation levels	One-way ANOVA	$F_{(6,65)} = 2.034$	$p = 0.0736$
SKF81297 effect in each subregion			
Subregion (1): control vs SKF	Paired *t* test	$t_{(10)} = 7.17$	$p < 0.001$
Subregion (2-1): control vs SKF	*t* test (Welch's-correction)	$t_{(10.09)} = 11.13$	$p < 0.001$
Subregion (2-2): control vs SKF	*t* test (Welch's-correction)	$t_{(10.69)} = 7.806$	$p < 0.001$
Subregion (2-3): control vs SKF	*t* test (Welch's-correction)	$t_{(11.77)} = 3.531$	$p = 0.0043$
Subregion (3): control vs SKF	*t* test (Welch's-correction)	$t_{(19.93)} = 1.136$	$p = 0.2696$
Subregion (4): control vs SKF	*t* test (Welch's-correction)	$t_{(11.77)} = 3.527$	$p = 0.0043$
Subregion (5): control vs SKF	*t* test (Welch's-correction)	$t_{(5.266)} = 4.053$	$p = 0.0088$
Two-way ANOVA for mediolateral axis			
SKF effect	Two-way ANOVA	$F_{(1,60)} = 164.1$	$p < 0.001$
Subregion effect	Two-way ANOVA	$F_{(2,60)} = 33.82$	$p < 0.001$
SKF-subregion interaction	Two-way ANOVA	$F_{(2,60)} = 22.72$	$p < 0.001$
SKF: subregion (2-1) vs (2-2)	Bonferroni *post hoc* test		$p < 0.001$
SKF: subregion (2-1) vs (2-3)	Bonferroni *post hoc* test		$p < 0.001$
SKF: subregion (2-2) vs (2-3)	Bonferroni *post hoc* test		$p < 0.001$
C, P-Thr202/Tyr204 ERK2/ERK2			
The basal phosphorylation levels	One-way ANOVA	$F_{(6,59)} = 1.981$	$p = 0.0828$
SKF81297 effect in each subregion			
Subregion (1): control vs SKF	Paired *t* test	$t_{(9)} = 3.559$	$p = 0.0061$
Subregion (2-1): control vs SKF	*t* test (Welch's-correction)	$t_{(7.565)} = 11.53$	$p < 0.001$
Subregion (2-2): control vs SKF	*t* test (Welch's-correction)	$t_{(15.75)} = 3.762$	$p = 0.0017$
Subregion (2-3): control vs SKF	*t* test (Welch's-correction)	$t_{(17.89)} = 2.292$	$p = 0.0343$
Subregion (3): control vs SKF	*t* test (Welch's-correction)	$t_{(16.42)} = 1.851$	$p = 0.0822$
Subregion (4): control vs SKF	*t* test (Welch's-correction)	$t_{(17.3)} = 3.372$	$p = 0.0036$
Subregion (5): control vs SKF	*t* test (Welch's-correction)	$t_{(5.302)} = 3.042$	$p = 0.0266$
Two-way ANOVA for mediolateral axis			
SKF effect	Two-way ANOVA	$F_{(2,60)} = 33.82$	$p < 0.001$
Subregion effect	Two-way ANOVA	$F_{(2,54)} = 2.255$	$p = 0.1147$
SKF-subregion interaction	Two-way ANOVA	$F_{(2,54)} = 6.35$	$p = 0.0033$
SKF: subregion (2-1) vs (2-2)	Bonferroni *post hoc* test		$p = 0.011$
SKF: subregion (2-1) vs (2-3)	Bonferroni *post hoc* test		$p = 0.0017$
SKF: subregion (2-2) vs (2-3)	Bonferroni *post hoc* test		$p > 0.9999$
D, P-Ser845 GluA1/GluA1			
Two-way ANOVA for subregion (1)			
SKF effect	Two-way ANOVA	$F_{(1,36)} = 22.37$	$p < 0.001$
Gene effect	Two-way ANOVA	$F_{(1,36)} = 4.878$	$p = 0.0336$

(*Table continues*.)

Table 1. Continued

Set of data	Type of statistical analysis	Results of statistical analysis	
SKF-gene interaction	Two-way ANOVA	$F_{(1,36)} = 2.111$	$p = 0.1549$
SKF: WT vs D32 KO	Bonferroni *post hoc* test		$p = 0.0276$
Two-way ANOVA for subregion (2-1)			
SKF effect	Two-way ANOVA	$F_{(1,32)} = 67.62$	$p < 0.001$
Gene effect	Two-way ANOVA	$F_{(1,32)} = 14.18$	$p = 0.0007$
SKF-gene interaction	Two-way ANOVA	$F_{(1,32)} = 9.843$	$p = 0.0036$
SKF: WT vs D32 KO	Bonferroni *post hoc* test		$p < 0.001$
Two-way ANOVA for subregion (2-2)			
SKF effect	Two-way ANOVA	$F_{(1,32)} = 52.03$	$p < 0.001$
Gene effect	Two-way ANOVA	$F_{(1,32)} = 15.86$	$p < 0.001$
SKF-gene interaction	Two-way ANOVA	$F_{(1,32)} = 8.812$	$p = 0.0056$
SKF: WT vs D32 KO	Bonferroni *post hoc* test		$p < 0.001$
Two-way ANOVA for subregion (2-3)			
SKF effect	Two-way ANOVA	$F_{(1,34)} = 39.76$	$p < 0.001$
Gene effect	Two-way ANOVA	$F_{(1,34)} = 9.552$	$p < 0.001$
SKF-gene interaction	Two-way ANOVA	$F_{(1,34)} = 8.231$	$p = 0.0070$
SKF: WT vs D32 KO	Bonferroni *post hoc* test		$p < 0.001$
Two-way ANOVA for subregion (3)			
SKF effect	Two-way ANOVA	$F_{(1,34)} = 21.31$	$p < 0.001$
Gene effect	Two-way ANOVA	$F_{(1,34)} = 7.965$	$p = 0.0079$
SKF-gene interaction	Two-way ANOVA	$F_{(1,34)} = 3.129$	$p = 0.0829$
SKF: WT vs D32 KO	Bonferroni *post hoc* test		$p = 0.0051$
Two-way ANOVA for subregion (4)			
SKF effect	Two-way ANOVA	$F_{(1,34)} = 35.67$	$p < 0.001$
Gene effect	Two-way ANOVA	$F_{(1,34)} = 14.77$	$p < 0.001$
SKF-gene interaction	Two-way ANOVA	$F_{(1,34)} = 10.4$	$p = 0.0028$
SKF: WT vs D32 KO	Bonferroni *post hoc* test		$p < 0.001$
Two-way ANOVA for subregion (5)			
SKF effect	Two-way ANOVA	$F_{(1,36)} = 27.56$	$p < 0.001$
Gene effect	Two-way ANOVA	$F_{(1,36)} = 5.488$	$p = 0.0248$
SKF-gene interaction	Two-way ANOVA	$F_{(1,36)} = 1.405$	$p = 0.2436$
SKF: WT vs D32 KO	Bonferroni *post hoc* test		$p = 0.0347$
E, P-Thr34 D32/D32			
The basal phosphorylation levels	One-way ANOVA	$F_{(6,53)} = 2.099$	$p = 0.0687$
Quinpirole effect in each subregion			
Subregion (1): control vs quinpirole	Paired *t* test	$t_{(8)} = 15.21$	$p < 0.001$
Subregion (2-1): control vs quinpirole	*t* test (Welch's-correction)	$t_{(11.62)} = 6.233$	$p < 0.001$
Subregion (2-2): control vs quinpirole	*t* test (Welch's-correction)	$t_{(14.04)} = 2.361$	$p = 0.0332$
Subregion (2-3): control vs quinpirole	*t* test (Welch's-correction)	$t_{(13.84)} = 3.655$	$p = 0.0026$
Subregion (3): control vs quinpirole	*t* test (Welch's-correction)	$t_{(7.999)} = 3.162$	$p = 0.0133$
Subregion (4): control vs quinpirole	*t* test (Welch's-correction)	$t_{(15.08)} = 4.403$	$p < 0.001$
Subregion (5): control vs quinpirole	*t* test (Welch's-correction)	$t_{(7.377)} = 2.341$	$p = 0.0499$
F, P-Ser40 TH/TH			
The basal phosphorylation levels	One-way ANOVA	$F_{(6,47)} = 5.059$	$p < 0.001$
Control: subregion (5) vs (1)	Bonferroni *post hoc* test		$p = 0.0183$
Control: subregion (5) vs (2-1)	Bonferroni *post hoc* test		$p = 0.0136$
Control: subregion (5) vs (2-2)	Bonferroni *post hoc* test		$p < 0.001$
Control: subregion (5) vs (2-3)	Bonferroni *post hoc* test		$p < 0.001$
Control: subregion (5) vs (3)	Bonferroni *post hoc* test		$p < 0.001$
Control: subregion (5) vs (4)	Bonferroni *post hoc* test		$p = 0.0052$
Quinpirole effect in each subregion			
Subregion (1): control vs quinpirole	Paired *t* test	$t_{(7)} = 9.916$	$p < 0.001$
Subregion (2-1): control vs quinpirole	*t* test (Welch's-correction)	$t_{(11.36)} = 6.396$	$p < 0.001$
Subregion (2-2): control vs quinpirole	*t* test (Welch's-correction)	$t_{(10.5)} = 6.326$	$p < 0.001$

(*Table continues*.)

Table 1. Continued

Set of data	Type of statistical analysis	Results of statistical analysis	
Subregion (2-3): control vs quinpirole	*t* test (Welch's-correction)	$t_{(12.46)} = 6.294$	$p < 0.001$
Subregion (3): control vs quinpirole	*t* test (Welch's-correction)	$t_{(11.87)} = 8.953$	$p < 0.001$
Subregion (4): control vs quinpirole	*t* test (Welch's-correction)	$t_{(10.26)} = 6.822$	$p < 0.001$
Subregion (5): control vs quinpirole	*t* test (Welch's-correction)	$t_{(6.918)} = 4.94$	$p < 0.001$

KO, knock-out; WT, wild type.

Table 2. Statistical analysis for Figure 4

Set of data	Type of statistical analysis	Results of statistical analysis	
A, DARPP-32 protein expression			
All subregions	One-way ANOVA	$F_{(6,70)} = 11.06$	$p < 0.001$
Subregion (1) vs (4)	Bonferroni *post hoc* test	$t_{(70)} = 3.331$	$p = 0.0083$
Subregion (1) vs (5)	Bonferroni *post hoc* test	$t_{(70)} = 6.549$	$p < 0.001$
B, GluA1 protein expression			
All subregions	One-way ANOVA	$F_{(6,70)} = 2.738$	$p = 0.0190$
Subregion (1) vs (4)	Bonferroni *post hoc* test	$t_{(70)} = 3.49$	$p = 0.0050$
C, ERK2 protein expression			
All subregions	One-way ANOVA	$F_{(6,64)} = 11.9$	$p < 0.001$
Subregion (1) vs (2-1)	Bonferroni *post hoc* test	$t_{(64)} = 3.004$	$p = 0.0228$
Subregion (1) vs (2-3)	Bonferroni *post hoc* test	$t_{(64)} = 3.439$	$p = 0.0062$
Subregion (1) vs (5)	Bonferroni *post hoc* test	$t_{(64)} = 4.914$	$p < 0.001$
Mediolateral axis	One-way ANOVA	$F_{(2,24)} = 9.668$	$p < 0.001$
Subregion (2-1) vs (2-3)	Bonferroni *post hoc* test	$t_{(24)} = 4.384$	$p < 0.001$
D, TH protein expression			
All subregions	One-way ANOVA	$F_{(6,70)} = 9.232$	$p < 0.001$
Subregion (1) vs (4)	Bonferroni *post hoc* test	$t_{(70)} = 5.767$	$p < 0.001$
Subregion (1) vs (5)	Bonferroni *post hoc* test	$t_{(70)} = 3.42$	$p = 0.0063$
J, ERK2 protein expression			
Subregion (1): unlesioned vs lesioned	Paired *t* test	$t_{(12)} = 3.319$	$p = 0.0061$

Table 3. Statistical analysis for Figure 5

Set of data	Type of statistical analysis	Results of statistical analysis	
A, P-Thr34 D32/D32			
The basal phosphorylation levels	One-way ANOVA	$F_{(6,41)} = 1.252$	$p = 0.0304$
CGS21680 effect in each subregion			
Subregion (1): control vs CGS	Paired *t* test	$t_{(6)} = 4.821$	$p = 0.0029$
Subregion (2-1): control vs CGS	*t* test (Welch's-correction)	$t_{(6.548)} = 3.158$	$p = 0.0174$
Subregion (2-2): control vs CGS	*t* test (Welch's-correction)	$t_{(6.429)} = 6.529$	$p < 0.001$
Subregion (2-3): control vs CGS	*t* test (Welch's-correction)	$t_{(6.668)} = 2.914$	$p = 0.0238$
Subregion (3): control vs CGS	*t* test (Welch's-correction)	$t_{(6.14)} = 2.563$	$p = 0.0419$
Subregion (4): control vs CGS	*t* test (Welch's-correction)	$t_{(7.008)} = 2.962$	$p = 0.0210$
Subregion (5): control vs CGS	*t* test (Welch's-correction)	$t_{(7.251)} = 3.012$	$p = 0.0188$
Two-way ANOVA for all subregions			
CGS effect	Two-way ANOVA	$F_{(1,83)} = 84.32$	$p < 0.001$
Subregion effect	Two-way ANOVA	$F_{(6,83)} = 2.112$	$p = 0.0604$
CGS-subregion interaction	Two-way ANOVA	$F_{(6,83)} = 2.656$	$p = 0.0209$
CGS: subregion (1) vs (3)	Bonferroni *post hoc* test		$p = 0.0259$
CGS: subregion (1) vs (4)	Bonferroni *post hoc* test		$p < 0.001$
CGS: subregion (1) vs (5)	Bonferroni *post hoc* test		$p < 0.001$

Table 4. Statistical analysis for Figure 6

Set of data	Type of statistical analysis	Results of statistical analysis	
A, DRD1 protein expression			
All subregions	One-way ANOVA	$F_{(6,28)} = 8.234$	$p < 0.001$
Subregion (1) vs (4)	Bonferroni *post hoc* test	$t_{(28)} = 3.06$	$p = 0.0290$
Subregion (1) vs (5)	Bonferroni *post hoc* test	$t_{(28)} = 5.657$	$p < 0.001$
B, Gαolf protein expression			
All subregions	One-way ANOVA	$F_{(6,46)} = 20.39$	$p < 0.001$
Subregion (1) vs (2-2)	Bonferroni *post hoc* test	$t_{(46)} = 3.262$	$p = 0.0125$
Subregion (1) vs (2-3)	Bonferroni *post hoc* test	$t_{(46)} = 3.622$	$p = 0.0044$
Subregion (1) vs (3)	Bonferroni *post hoc* test	$t_{(46)} = 3.951$	$p = 0.0016$
Subregion (1) vs (5)	Bonferroni *post hoc* test	$t_{(46)} = 6.357$	$p < 0.001$
Mediolateral axis	One-way ANOVA	$F_{(2,15)} = 6.681$	$p = 0.0084$
Subregion (2-1) vs (2-2)	Bonferroni *post hoc* test	$t_{(15)} = 2.945$	$p = 0.0301$
Subregion (2-1) vs (2-3)	Bonferroni *post hoc* test	$t_{(15)} = 3.348$	$p = 0.0132$
C, PDE10A protein expression			
All subregions	One-way ANOVA	$F_{(6,46)} = 26.71$	$p < 0.001$
Subregion (1) vs (2-2)	Bonferroni *post hoc* test	$t_{(46)} = 2.869$	$p = 0.0372$
Subregion (1) vs (2-3)	Bonferroni *post hoc* test	$t_{(46)} = 5.701$	$p < 0.001$
Subregion (1) vs (3)	Bonferroni *post hoc* test	$t_{(46)} = 4.629$	$p < 0.001$
Subregion (1) vs (5)	Bonferroni *post hoc* test	$t_{(46)} = 6.497$	$p < 0.001$
Mediolateral axis	One-way ANOVA	$F_{(2,15)} = 19.8$	$p < 0.001$
Subregion (2-1) vs (2-2)	Bonferroni *post hoc* test	$t_{(15)} = 3.785$	$p = 0.0054$
Subregion (2-1) vs (2-3)	Bonferroni *post hoc* test	$t_{(15)} = 6.247$	$p < 0.001$
D, ChAT protein expression			
All subregions	One-way ANOVA	$F_{(6,46)} = 7.741$	$p < 0.001$
Subregion (1) vs (3)	Bonferroni *post hoc* test	$t_{(46)} = 3.566$	$p = 0.0052$
Subregion (1) vs (5)	Bonferroni *post hoc* test	$t_{(46)} = 3.062$	$p = 0.0220$

Svenningsson et al., 2004). The PKA/DARPP-32 signaling cascade plays an essential role in dopaminergic neurotransmission and behavioral responses to dopamine (Fienberg et al., 1998; Nishi et al., 2011).

Tyrosine hydroxylase (TH) is expressed abundantly at dopaminergic terminals and to a lesser extent in TH-positive interneurons in the striatum (Xenias et al., 2015). Activation of D2 autoreceptors at dopaminergic terminals reduces the phosphorylation of TH at Ser40 by PKA (Nishi et al., 2008), resulting in the inhibition of TH activity and dopamine synthesis.

Recent progress in comprehensive projectome and striosome mapping prompted us to investigate the regional differences in dopamine neurotransmission in the striatum. Based on corticostriatal connectivity and striosome maps (Hintiryan et al., 2016; Hunnicutt et al., 2016; Miyamoto et al., 2018), the striatum was subdivided into seven subregions. Pharmacological analyses identified subregions with low D1 receptor signaling. The contribution of subregion-specific regulation of D1 receptor signaling

Table 5. Statistical analysis for Figure 7

Set of data	Type of statistical analysis	Results of statistical analysis	
A, P-Thr34 D32/D32			
Papaverine effect in each subregion			
Subregion (1): control vs papaverine	Paired *t* test	$t_{(5)} = 5.006$	$p = 0.0041$
Subregion (2-1): control vs papaverine	*t* test (Welch's-correction)	$t_{(5.365)} = 6.137$	$p = 0.0013$
Subregion (2-2): control vs papaverine	*t* test (Welch's-correction)	$t_{(5.779)} = 7.555$	$p < 0.001$
Subregion (2-3): control vs papaverine	*t* test (Welch's-correction)	$t_{(5.074)} = 2.991$	$p = 0.028$
Subregion (3): control vs papaverine	*t* test (Welch's-correction)	$t_{(4.167)} = 5.067$	$p = 0.0085$
Subregion (4): control vs papaverine	*t* test (Welch's-correction)	$t_{(5.054)} = 4.356$	$p = 0.0071$
Subregion (5): control vs papaverine	*t* test (Welch's-correction)	$t_{(3.002)} = 4.181$	$p = 0.0249$
B, P-Ser845 GluA1/GluA1			
Papaverine effect in each subregion			
Subregion (1): control vs papaverine	Paired *t* test	$t_{(5)} = 5.298$	$p = 0.0032$
Subregion (2-1): control vs papaverine	*t* test (Welch's-correction)	$t_{(5.054)} = 5.967$	$p = 0.0018$
Subregion (2-2): control vs papaverine	*t* test (Welch's-correction)	$t_{(5.049)} = 5.41$	$p = 0.0028$
Subregion (2-3): control vs papaverine	*t* test (Welch's-correction)	$t_{(5.04)} = 4.896$	$p = 0.0044$
Subregion (3): control vs papaverine	*t* test (Welch's-correction)	$t_{(5.037)} = 6.561$	$p = 0.0012$
Subregion (4): control vs papaverine	*t* test (Welch's-correction)	$t_{(5.081)} = 5.127$	$p = 0.0035$
Subregion (5): control vs papaverine	*t* test (Welch's-correction)	$t_{(3.094)} = 4.5$	$p = 0.0192$
C, P-Thr34 D32/D32			
Homogenate			
Subregion (1): control vs papaverine	Paired *t* test	$t_{(5)} = 5.217$	$p = 0.0034$
Subregion (2-3): control vs papaverine	*t* test (Welch's-correction)	$t_{(5.132)} = 7.803$	$p < 0.001$
Subregion (3): control vs papaverine	*t* test (Welch's-correction)	$t_{(5.245)} = 6.065$	$p = 0.0015$
D1-Flag	Two-way ANOVA		
Subregion (1): control vs papaverine	Paired *t* test	$t_{(4)} = 3.762$	$p = 0.0197$
Subregion (2-3): control vs papaverine	*t* test (Welch's-correction)	$t_{(5.241)} = 10.71$	$p < 0.001$
Subregion (3): control vs papaverine	*t* test (Welch's-correction)	$t_{(4.383)} = 3.137$	$p = 0.0308$
Two-way ANOVA for D1-Flag			
Papaverine effect	Two-way ANOVA	$F_{(1,24)} = 56.48$	$p < 0.001$
Subregion effect	Two-way ANOVA	$F_{(2,24)} = 2.111$	$p = 0.1430$
Papaverine-subregion interaction	Two-way ANOVA	$F_{(2,24)} = 4.469$	$p = 0.0224$
Papaverine: subregion (1) vs (2-3)	Bonferroni *post hoc* test		$p = 0.0062$
Papaverine: subregion (1) vs (3)	Bonferroni *post hoc* test		$p = 0.0607$
D2-Myc	Two-way ANOVA		
Subregion (1): control vs papaverine	Paired *t* test	$t_{(4)} = 4.403$	$p = 0.0117$
Subregion (2-3): control vs papaverine	*t* test (Welch's-correction)	$t_{(8)} = 4.852$	$p = 0.0031$
Subregion (3): control vs papaverine	*t* test (Welch's-correction)	$t_{(8)} = 4.596$	$p = 0.0018$

to the pathophysiology of Parkinson's disease and L-DOPA-induced dyskinesia (LID) was further investigated.

Materials and Methods

Preparation, incubation, and processing of neostriatal slices

Male C57BL/6N mice at 9–15 weeks of age were purchased from Japan SLC. All mice used in this study were handled in accordance with the *Guide for the Care and Use of Laboratory Animals* as adopted by the National Institutes of Health. The Institutional Animal Care and Use Committee of Kurume University School of Medicine approved the specific protocols. Male C57BL/6N mice were killed by decapitation. The brains were rapidly removed and placed in ice-cold, oxygenated Krebs-HCO_3^- buffer (124 mM NaCl, 4 mM KCl, 26 mM $NaHCO_3$, 1.5 mM $CaCl_2$, 1.25 mM KH_2PO_4, 1.5 mM $MgSO_4$ and 10 mM D-glucose, pH 7.4). Coronal slices (350 μm) were prepared using a vibrating blade microtome, VT1000S (Leica Microsystems). Striatal slices were dissected from the slices in ice-cold Krebs-HCO_3^- buffer, and subdivided into seven subregions as described below. Each slice was placed in a polypropylene incubation tube with 2 ml of fresh Krebs-HCO_3^- buffer containing adenosine deaminase (10 μg/ml). The slices were preincubated at 30°C under constant oxygenation with 95% O_2/5% CO_2 for 60 min. The buffer was replaced with fresh Krebs-HCO_3^- buffer after 30 min of preincubation. Adenosine deaminase was included during the 60 min of preincubation. The slices were treated with drugs, as specified in each experiment. The drugs were obtained from the following sources: (±)−6-chloro-2,3,4,5-tetrahydro-1-phenyl-1*H*-3-benzazepine hydrobromide [(±)-SKF81297], quinpirole, papaverine and atropine from Sigma-Aldrich, and muscarinic toxin (MT3) from Peptide Institute. After drug treatment, slices were transferred to Eppendorf tubes, frozen on dry ice, and stored at −80°C until assayed.

Frozen tissue samples were sonicated in boiling 1% SDS containing 50 mM sodium fluoride and boiled for an additional 10 min. Small aliquots of the homogenate were retained for protein determination using the BCA protein assay method (Pierce). Equal amounts of protein were loaded onto 10% or 5–20% Extra PAGE One Precast Gel (Nacalai Tesque) or 10% SDS/polyacrylamide gel, separated by electrophoresis, and then transferred to nitrocellulose membranes (0.2 μm; Sigma-Aldrich).

In some experiments, neostriatal slices were prepared from C57BL/6J mice (9–15 weeks of age) lacking the gene for DARPP-32 (Fienberg et al., 1998). DARPP-32 knock-out and wild-type mice (C57BL/6J genetic

Table 6. Statistical analysis for Figure 8

Set of data	Type of statistical analysis	Results of statistical analysis	
A, P-Thr34 D32/D32			
Subregion (1): control vs atropine	*t* test	$t_{(6)} = 0.07706$	$p = 0.9411$
Subregion (1): control vs MT3	*t* test	$t_{(12)} = 1.341$	$p = 0.2048$
A, P-Ser845 GluA1/GluA1			
Subregion (1): control vs atropine	*t* test	$t_{(6)} = 1.495$	$p = 0.1856$
Subregion (1): control vs MT3	*t* test	$t_{(12)} = 1.173$	$p = 0.2634$
B, P-Thr34 D32/D32			
Subregion (1)	One-way ANOVA	$F_{(3,28)} = 24.06$	$p < 0.001$
Atropine vs atropine+SKF	Bonferroni *post hoc* test		$p < 0.001$
SKF vs atropine+SKF	Bonferroni *post hoc* test		$p = 0.0013$
Atropine vs atropine+SKF	Newman–Keuls *post hoc* test		$p < 0.001$
SKF vs atropine+SKF	Newman–Keuls *post hoc* test		$p < 0.001$
Subregion (2-1)	One-way ANOVA	$F_{(3,28)} = 12.74$	$p < 0.001$
Atropine vs atropine+SKF	Bonferroni *post hoc* test		$p = 0.0034$
SKF vs atropine+SKF	Bonferroni *post hoc* test		$p > 0.9999$
Atropine vs atropine+SKF	Newman–Keuls *post hoc* test		$p < 0.01$
SKF vs atropine+SKF	Newman–Keuls *post hoc* test		n.s.
Subregion (2-2)	One-way ANOVA	$F_{(3,28)} = 10.26$	$p < 0.001$
Atropine vs atropine+SKF	Bonferroni *post hoc* test		$p = 0.0040$
SKF vs atropine+SKF	Bonferroni *post hoc* test		$p > 0.9999$
Atropine vs atropine+SKF	Newman–Keuls *post hoc* test		$p < 0.01$
SKF vs atropine+SKF	Newman–Keuls *post hoc* test		n.s.
Subregion (2-3)	One-way ANOVA	$F_{(3,28)} = 21.52$	$p < 0.001$
Atropine vs atropine+SKF	Bonferroni *post hoc* test		$p < 0.001$
SKF vs atropine+SKF	Bonferroni *post hoc* test		$p = 0.0167$
Atropine vs atropine+SKF	Newman–Keuls *post hoc* test		$p < 0.001$
SKF vs atropine+SKF	Newman–Keuls *post hoc* test		$p < 0.01$
Subregion (3)	One-way ANOVA	$F_{(3,28)} = 18.49$	$p < 0.001$
Atropine vs atropine+SKF	Bonferroni *post hoc* test		$p < 0.001$
SKF vs atropine+SKF	Bonferroni *post hoc* test		$p < 0.001$
Atropine vs atropine+SKF	Newman–Keuls *post hoc* test		$p < 0.001$
SKF vs atropine+SKF	Newman–Keuls *post hoc* test		$p < 0.001$
Subregion (4)	One-way ANOVA	$F_{(3,28)} = 14.62$	$p < 0.001$
Atropine vs atropine+SKF	Bonferroni *post hoc* test		$p < 0.001$
SKF vs atropine+SKF	Bonferroni *post hoc* test		$p = 0.0057$
Atropine vs atropine+SKF	Newman–Keuls *post hoc* test		$p < 0.001$
SKF vs atropine+SKF	Newman–Keuls *post hoc* test		$p < 0.001$
Subregion (5)	One-way ANOVA	$F_{(3,18)} = 10.17$	$p < 0.001$
Atropine vs atropine+SKF	Bonferroni *post hoc* test		$p = 0.0022$
SKF vs atropine+SKF	Bonferroni *post hoc* test		$p = 0.2773$
Atropine vs atropine+SKF	Newman–Keuls *post hoc* test		$p < 0.01$
SKF vs atropine+SKF	Newman–Keuls *post hoc* test		$p < 0.05$
C, P-Ser845 GluA1/GluA1			
Subregion (1)	One-way ANOVA	$F_{(3,28)} = 34.32$	$p < 0.001$
Atropine vs atropine+SKF	Bonferroni *post hoc* test		$p = 0.0001$
SKF vs atropine+SKF	Bonferroni *post hoc* test		$p < 0.001$
Atropine vs atropine+SKF	Newman–Keuls *post hoc* test		$p < 0.001$
SKF vs atropine+SKF	Newman–Keuls *post hoc* test		$p < 0.001$
Subregion (2-1)	One-way ANOVA	$F_{(3,28)} = 35.42$	$p < 0.001$
Atropine vs atropine+SKF	Bonferroni *post hoc* test		$p < 0.001$
SKF vs atropine+SKF	Bonferroni *post hoc* test		$p = 0.9533$
Atropine vs atropine+SKF	Newman–Keuls *post hoc* test		$p < 0.001$
SKF vs atropine+SKF	Newman–Keuls *post hoc* test		n.s.
Subregion (2-2)	One-way ANOVA	$F_{(3,28)} = 23.08$	$p < 0.001$
Atropine vs atropine+SKF	Bonferroni *post hoc* test		$p < 0.001$
SKF vs atropine+SKF	Bonferroni *post hoc* test		$\mathbf{p = 0.0884}$
Atropine vs atropine+SKF	Newman–Keuls *post hoc* test		$p < 0.001$
SKF vs atropine+SKF	Newman–Keuls *post hoc* test		$\mathbf{p < 0.05}$
Subregion (2-3)	One-way ANOVA	$F_{(3,28)} = 11.91$	$p < 0.001$
Atropine vs atropine+SKF	Bonferroni *post hoc* test		$p < 0.001$
SKF vs atropine+SKF	Bonferroni *post hoc* test		$\mathbf{p = 0.1295}$
Atropine vs atropine+SKF	Newman–Keuls *post hoc* test		$p < 0.001$
SKF vs atropine+SKF	Newman–Keuls *post hoc* test		$\mathbf{p < 0.05}$
Subregion (3)	One-way ANOVA	$F_{(3,28)} = 19.94$	$p < 0.001$
Atropine vs atropine+SKF	Bonferroni *post hoc* test		$p < 0.001$
SKF vs atropine+SKF	Bonferroni *post hoc* test		$p < 0.001$
Atropine vs atropine+SKF	Newman–Keuls *post hoc* test		$p < 0.001$
SKF vs atropine+SKF	Newman–Keuls *post hoc* test		$p < 0.001$
Subregion (4)	One-way ANOVA	$F_{(3,28)} = 9.299$	$p < 0.001$
Atropine vs atropine+SKF	Bonferroni *post hoc* test		$p = 0.0036$
SKF vs atropine+SKF	Bonferroni *post hoc* test		$p > 0.9999$
Atropine vs atropine+SKF	Newman–Keuls *post hoc* test		$p < 0.01$
SKF vs atropine+SKF	Newman–Keuls *post hoc* test		n.s.
Subregion (5)	One-way ANOVA	$F_{(3,18)} = 10.44$	$p < 0.001$
Atropine vs atropine+SKF	Bonferroni *post hoc* test		$p = 0.0024$
SKF vs atropine+SKF	Bonferroni *post hoc* test		$p > 0.9999$
Atropine vs atropine+SKF	Newman–Keuls *post hoc* test		$p < 0.01$
SKF vs atropine+SKF	Newman–Keuls *post hoc* test		n.s.
D, P-Thr34 D32/D32			
Subregion (1)	One-way ANOVA	$F_{(3,32)} = 14.16$	$p < 0.001$
MT3 vs MT3+SKF	Bonferroni *post hoc* test		$p < 0.001$
SKF vs MT3+SKF	Bonferroni *post hoc* test		$p = 0.0171$
MT3 vs MT3+SKF	Newman–Keuls *post hoc* test		$p < 0.001$
SKF vs MT3+SKF	Newman–Keuls *post hoc* test		$p < 0.01$
Subregion (2-1)	One-way ANOVA	$F_{(3,34)} = 6.9076$	$p < 0.001$
MT3 vs MT3+SKF	Bonferroni *post hoc* test		$p = 0.0094$
SKF vs MT3+SKF	Bonferroni *post hoc* test		$p > 0.9999$
MT3 vs MT3+SKF	Newman–Keuls *post hoc* test		$p < 0.01$
SKF vs MT3+SKF	Newman–Keuls *post hoc* test		n.s.
Subregion (2-2)	One-way ANOVA	$F_{(3,34)} = 6.964$	$p < 0.001$

(*Table continues*.)

Table 6. Continued

Set of data	Type of statistical analysis	Results of statistical analysis	
MT3 vs MT3+SKF	Bonferroni *post hoc* test		$p = 0.0033$
SKF vs MT3+SKF	Bonferroni *post hoc* test		$\mathbf{p = 0.1520}$
MT3 vs MT3+SKF	Newman–Keuls *post hoc* test		$p < 0.01$
SKF vs MT3+SKF	Newman–Keuls *post hoc* test		$\mathbf{p < 0.05}$
Subregion (2-3)	One-way ANOVA	$F_{(3,34)} = 16.52$	$p < 0.001$
MT3 vs MT3+SKF	Bonferroni *post hoc* test		$p < 0.001$
SKF vs MT3+SKF	Bonferroni *post hoc* test		$\mathbf{p = 0.1756}$
MT3 vs MT3+SKF	Newman–Keuls *post hoc* test		$p < 0.001$
SKF vs MT3+SKF	Newman–Keuls *post hoc* test		$\mathbf{p < 0.05}$
Subregion (3)	One-way ANOVA	$F_{(3,34)} = 6.887$	$p < 0.001$
MT3 vs MT3+SKF	Bonferroni *post hoc* test		$p = 0.0019$
SKF vs MT3+SKF	Bonferroni *post hoc* test		$p = 0.1136$
MT3 vs MT3+SKF	Newman–Keuls *post hoc* test		$p < 0.01$
SKF vs MT3+SKF	Newman–Keuls *post hoc* test		$\mathbf{p < 0.05}$
Subregion (4)	One-way ANOVA	$F_{(3,34)} = 7.428$	$p < 0.001$
MT3 vs MT3+SKF	Bonferroni *post hoc* test		$p = 0.0023$
SKF vs MT3+SKF	Bonferroni *post hoc* test		$\mathbf{p = 0.1630}$
MT3 vs MT3+SKF	Newman–Keuls *post hoc* test		$p < 0.01$
SKF vs MT3+SKF	Newman–Keuls *post hoc* test		$\mathbf{p < 0.05}$
Subregion (5)	One-way ANOVA	$F_{(3,24)} = 7.968$	$p < 0.001$
MT3 vs MT3+SKF	Bonferroni *post hoc* test		$p = 0.0019$
SKF vs MT3+SKF	Bonferroni *post hoc* test		$p = 0.0276$
MT3 vs MT3+SKF	Newman–Keuls *post hoc* test		$p < 0.001$
SKF vs MT3+SKF	Newman–Keuls *post hoc* test		$p < 0.01$
E, P-Ser845 GluA1/GluA1			
Subregion (1)	One-way ANOVA	$F_{(3,32)} = 53.09$	$p < 0.001$
MT3 vs MT3+SKF	Bonferroni *post hoc* test		$p < 0.001$
SKF vs MT3+SKF	Bonferroni *post hoc* test		$p < 0.001$
MT3 vs MT3+SKF	Newman–Keuls *post hoc* test		$p < 0.001$
SKF vs MT3+SKF	Newman–Keuls *post hoc* test		$p < 0.001$
Subregion (2-1)	One-way ANOVA	$F_{(3,34)} = 38.64$	$p < 0.001$
MT3 vs MT3+SKF	Bonferroni *post hoc* test		$p < 0.001$
SKF vs MT3+SKF	Bonferroni *post hoc* test		$\mathbf{p = 0.2357}$
MT3 vs MT3+SKF	Newman–Keuls *post hoc* test		$p < 0.001$
SKF vs MT3+SKF	Newman–Keuls *post hoc* test		$\mathbf{p < 0.05}$
Subregion (2-2)	One-way ANOVA	$F_{(3,34)} = 52.18$	$p < 0.001$
MT3 vs MT3+SKF	Bonferroni *post hoc* test		$p < 0.001$
SKF vs MT3+SKF	Bonferroni *post hoc* test		$p < 0.001$
MT3 vs MT3+SKF	Newman–Keuls *post hoc* test		$p < 0.001$
SKF vs MT3+SKF	Newman–Keuls *post hoc* test		$p < 0.001$
Subregion (2-3)	One-way ANOVA	$F_{(3,34)} = 20.72$	$p < 0.001$
MT3 vs MT3+SKF	Bonferroni *post hoc* test		$p < 0.001$
SKF vs MT3+SKF	Bonferroni *post hoc* test		$p = 0.0045$
MT3 vs MT3+SKF	Newman–Keuls *post hoc* test		$p < 0.001$
SKF vs MT3+SKF	Newman–Keuls *post hoc* test		$p < 0.001$
Subregion (3)	One-way ANOVA	$F_{(3,34)} = 24.11$	$p < 0.001$
MT3 vs MT3+SKF	Bonferroni *post hoc* test		$p < 0.001$
SKF vs MT3+SKF	Bonferroni *post hoc* test		$p < 0.001$
MT3 vs MT3+SKF	Newman–Keuls *post hoc* test		$p < 0.001$
SKF vs MT3+SKF	Newman–Keuls *post hoc* test		$p < 0.001$
Subregion (4)	One-way ANOVA	$F_{(3,34)} = 16.6$	$p < 0.001$
MT3 vs MT3+SKF	Bonferroni *post hoc* test		$p < 0.001$
SKF vs MT3+SKF	Bonferroni *post hoc* test		$p = 0.045$
MT3 vs MT3+SKF	Newman–Keuls *post hoc* test		$p < 0.01$
SKF vs MT3+SKF	Newman–Keuls *post hoc* test		$p < 0.001$
Subregion (5)	One-way ANOVA	$F_{(3,24)} = 35.95$	$p < 0.001$
MT3 vs MT3+SKF	Bonferroni *post hoc* test		$p < 0.001$
SKF vs MT3+SKF	Bonferroni *post hoc* test		$p < 0.001$
MT3 vs MT3+SKF	Newman–Keuls *post hoc* test		$p < 0.001$
SKF vs MT3+SKF	Newman–Keuls *post hoc* test		$p < 0.001$

P-values marked with boldface indicate statistically significant differences with Newman-Keuls post hoc test, but not with Bonferroni post hoc test. n.s., not significant.

background) were generated from the offspring of homozygous and wild-type mating pairs, respectively.

Striatal subregions

Striatal slices prepared from 1.54 to −1.26 mm anterior to the bregma were divided into four rostrocaudal levels: rostral (R), intermediate/rostral (IR), intermediate/caudal (IC), and caudal (C) parts of the striatum (Fig. 1). Rostrocaudal levels were determined by the anterior commissure crossing the midline, positioned at 0.14 mm anterior to the bregma (Miyamoto et al., 2018). Striatal slices at the second rostral level [subregion (2); IR part] were further divided into three mediolateral portions: medial, central, and dorsolateral portions, which corresponded to intrastriatal domains of the μ-opioid receptor (+)/substance P (+) striosome, μ-opioid receptor (+) striosome, and striosome-free space, respectively (Miyamoto et al., 2018). Slices of the NAc [subregion (5)] were dissected from the ventral parts of slices at the rostral level [subregion (1)]. Accordingly, striatal slices (1.54 to −1.26 mm anterior to the bregma) were divided into seven subregions (Fig. 1): (1) the R part (1.54–0.84 mm); (2) the IR part, subdivided into (2-1) medial (M-IR), (2-2) central (C-IR), and (2-3) dorsolateral (DL-IR) portions (0.84–0.14 mm); (3) the IC part (0.14 to −0.56 mm); (4) the C part (−0.56 to −1.26 mm); and (5) the NAc (1.54–0.84 mm). Two sequential slices were used for analysis in each subregion.

Immunoblotting

The membranes were immunoblotted using phosphorylation state-specific antibodies raised against phosphopeptides: phospho-Thr34 DARPP-32, a site phosphorylated by PKA (D27A4, 1:1000 dilution, Cell Signaling Technology); phospho-Ser845 GluA1, a site phosphorylated by PKA (p1160-845, 1:250 dilution, PhosphoSolutions); phospho-Thr202/Tyr204 ERK, a site phosphorylated by MEK (#9101, 1:5000 dilution, Cell Signaling Technology); and phospho-Ser40 TH, a site phosphorylated by PKA (ab51206, 1:250 dilution, Abcam). Antibodies generated against DARPP-32 (C24-5a, 1:20 000 dilution, The Rockefeller University), GulA1 (E-6, 1:250 dilution, Santa Cruz Biotechnology), ERK (#9102, 1:1000 dilution, New England BioLabs), TH (TH-16, 1:5000 dilution, Sigma-Aldrich), dopamine D1 receptor (DRD1; D2944, 1:1200 dilution, Sigma-Aldrich), phosphodiesterase 10A (PDE10A; NB300-645, 1:500 dilution, Novus Biologicals), choline acetyltransferase (ChAT; #AB144P, 1:1000 dilution, Merck Millipore), and β-actin (#4970, 1:1000 dilution, Cell Signaling Technology; 66009-1-Ig, 1:1000 dilution, Proteintech) were used to determine the total amount of proteins. None of the

Table 7. Statistical analysis for Figure 9

Set of data	Type of statistical analysis	Results of statistical analysis	
A, pole test			
Day 1 vs day 15	*t* test (Welch's-correction)	$t_{(10.08)} = 3.161$	$p < 0.05$
A, cylinder test			
Day 1 vs day 15	*t* test	$t_{(20)} = 3.657$	$p < 0.01$
B, P-Thr34 D32/D32			
Two-way ANOVA for subregion (1)			
SKF effect	Two-way ANOVA	$F_{(1,24)} = 16.07$	$p < 0.001$
6-OHDA effect	Two-way ANOVA	$F_{(1,24)} = 7.827$	$p = 0.0100$
SKF-6-OHDA interaction	Two-way ANOVA	$F_{(1,24)} = 6.299$	$p = 0.0192$
SKF: unlesioned side vs lesioned side	Bonferroni *post hoc* test		$p < 0.001$
Two-way ANOVA for subregion (2-1)			
SKF effect	Two-way ANOVA	$F_{(1,22)} = 18.28$	$p < 0.001$
6-OHDA effect	Two-way ANOVA	$F_{(1,22)} = 3.859$	$p = 0.0619$
SKF-6-OHDA interaction	Two-way ANOVA	$F_{(1,22)} = 4.129$	$p = 0.0527$
SKF: unlesioned side vs lesioned side	Bonferroni *post hoc* test		$p = 0.0147$
Two-way ANOVA for subregion (2-2)			
SKF effect	Two-way ANOVA	$F_{(1,20)} = 33.1$	$p < 0.001$
6-OHDA effect	Two-way ANOVA	$F_{(1,20)} = 6.996$	$p = 0.0155$
SKF-6-OHDA interaction	Two-way ANOVA	$F_{(1,20)} = 7.672$	$p = 0.0118$
SKF: unlesioned side vs lesioned side	Bonferroni *post hoc* test		$p = 0.0021$
Two-way ANOVA for subregion (2-3)			
SKF effect	Two-way ANOVA	$F_{(1,21)} = 20.19$	$p < 0.001$
6-OHDA effect	Two-way ANOVA	$F_{(1,21)} = 10.39$	$p = 0.0041$
SKF-6-OHDA interaction	Two-way ANOVA	$F_{(1,21)} = 6.634$	$p = 0.0176$
SKF: unlesioned side vs lesioned side	Bonferroni *post hoc* test		$p < 0.001$
Two-way ANOVA for subregion (4)			
SKF effect	Two-way ANOVA	$F_{(1,24)} = 14.44$	$p < 0.001$
6-OHDA effect	Two-way ANOVA	$F_{(1,24)} = 3.12$	$p = 0.0901$
SKF-6-OHDA interaction	Two-way ANOVA	$F_{(1,24)} = 2.282$	$p = 0.1439$
SKF: unlesioned side vs lesioned side	Bonferroni *post hoc* test		$p = 0.0391$
C, P-Ser845 GluA1/GluA1			
Two-way ANOVA for subregion (1)			
SKF effect	Two-way ANOVA	$F_{(1,24)} = 16.83$	$p < 0.001$
6-OHDA effect	Two-way ANOVA	$F_{(1,24)} = 3.93$	$p = 0.0590$
SKF-6-OHDA interaction	Two-way ANOVA	$F_{(1,24)} = 6.095$	$p = 0.0211$
SKF: unlesioned side vs lesioned side	Bonferroni *post hoc* test		$p = 0.0047$
Two-way ANOVA for subregion (2-1)			
SKF effect	Two-way ANOVA	$F_{(1,22)} = 40.51$	$p < 0.001$
6-OHDA effect	Two-way ANOVA	$F_{(1,22)} = 6.325$	$p = 0.0197$
SKF-6-OHDA interaction	Two-way ANOVA	$F_{(1,22)} = 8.508$	$p = 0.0080$
SKF: unlesioned side vs lesioned side	Bonferroni *post hoc* test		$p = 0.0012$
Two-way ANOVA for subregion (2-2)			
SKF effect	Two-way ANOVA	$F_{(1,20)} = 24.45$	$p < 0.001$
6-OHDA effect	Two-way ANOVA	$F_{(1,20)} = 2.927$	$p = 0.1026$
SKF-6-OHDA interaction	Two-way ANOVA	$F_{(1,20)} = 6.822$	$p = 0.0167$
SKF: unlesioned side vs lesioned side	Bonferroni *post hoc* test		$p = 0.0125$
Two-way ANOVA for subregion (2-3)			
SKF effect	Two-way ANOVA	$F_{(1,21)} = 23.25$	$p < 0.001$
6-OHDA effect	Two-way ANOVA	$F_{(1,21)} = 5.841$	$p = 0.0248$
SKF-6-OHDA interaction	Two-way ANOVA	$F_{(1,21)} = 8.255$	$p = 0.0091$
SKF: unlesioned side vs lesioned side	Bonferroni *post hoc* test		$p = 0.0020$
D, P-Thr202/Tyr204 ERK2/ERK2			
Two-way ANOVA for subregion (1)			

(*Table continues*.)

Table 7. Continued

Set of data	Type of statistical analysis	Results of statistical analysis	
SKF effect	Two-way ANOVA	$F_{(1,24)} = 29.83$	$p < 0.001$
6-OHDA effect	Two-way ANOVA	$F_{(1,24)} = 4.401$	$p = 0.0558$
SKF-6-OHDA interaction	Two-way ANOVA	$F_{(1,24)} = 8.406$	$p = 0.0079$
SKF: unlesioned side vs lesioned side	Bonferroni *post hoc* test		$p = 0.0020$
Two-way ANOVA for subregion (2-2)			
SKF effect	Two-way ANOVA	$F_{(1,20)} = 35.53$	$p < 0.001$
6-OHDA effect	Two-way ANOVA	$F_{(1,20)} = 2.216$	$p = 0.1522$
SKF-6-OHDA interaction	Two-way ANOVA	$F_{(1,20)} = 3.896$	$p = 0.0624$
SKF: unlesioned side vs lesioned side	Bonferroni *post hoc* test		$p = 0.0474$

Table 8. Statistical analysis for Figure 11

Set of data	Type of statistical analysis	Results of statistical analysis	
B, Gαolf protein expression			
Subregion (1): unlesioned vs lesioned	Paired *t* test	$t_{(13)} = 3.461$	$p = 0.0042$
Subregion (2-1): unlesioned vs lesioned	*t* test (Welch's-correction)	$t_{(21.56)} = 3.097$	$p = 0.0053$
C, PDE10A protein expression			
Subregion (1): unlesioned vs lesioned	Paired *t* test	$t_{(13)} = 3.676$	$p = 0.0028$
D, ChAT protein expression			
Subregion (1): unlesioned vs lesioned	Paired *t* test	$t_{(12)} = 2.631$	$p = 0.0234$
F, Gαolf protein expression			
Subregion (1): unlesioned vs lesioned	Paired *t* test	$t_{(12)} = 2.605$	$p = 0.0230$
Subregion (2-1): unlesioned vs lesioned	*t* test (Welch's-correction)	$t_{(21.45)} = 3.602$	$p = 0.0016$
Subregion (2-2): unlesioned vs lesioned	*t* test (Welch's-correction)	$t_{(23.49)} = 2.649$	$p = 0.0142$
Subregion (3): unlesioned vs lesioned	*t* test (Welch's-correction)	$t_{(22.91)} = 3.116$	$p = 0.0049$
G, PDE10A protein expression			
Subregion (1): unlesioned vs lesioned	Paired *t* test	$t_{(12)} = 2.919$	$p = 0.0129$
Subregion (2-3): unlesioned vs lesioned	*t* test (Welch's-correction)	$t_{(22.62)} = 3.064$	$p = 0.0056$
Subregion (4): unlesioned vs lesioned	*t* test (Welch's-correction)	$t_{(24)} = 2.142$	$p = 0.0426$
H, ChAT protein expression			
Subregion (1): unlesioned vs lesioned	Paired *t* test	$t_{(12)} = 2.533$	$p = 0.0263$
Subregion (2-1): unlesioned vs lesioned	*t* test (Welch's-correction)	$t_{(16.86)} = 3.243$	$p = 0.0048$

experimental slice manipulations used in the present study altered the total levels of specific phosphoproteins. Signal intensities were normalized with β-actin and the proportion of DARPP-32-positive areas in each subregion of the striatum (see DARPP-32 immunohistochemistry).

The membrane was incubated with a donkey anti-goat or a goat anti-mouse or rabbit Alexa 680-linked IgG (1:5000 dilution, Thermo Fisher Scientific) or a goat anti-mouse or rabbit IRDye800-linked IgG (1:5000 dilution, Thermo Fisher Scientific). Fluorescence at infrared wavelengths was detected by the Odyssey infrared imaging system (LI-COR) and quantified using the Odyssey software.

DARPP-32 immunohistochemistry

Male C57BL/6N mice at 9–11 weeks of age were perfused through the left ventricle with 4% paraformaldehyde, as described previously (Nishi et al., 2008). Serial coronal sections 50 μm in thickness were cut with a vibrating microtome, VT1000S (Leica Microsystems). Sections were processed for immunohistochemistry using the free-floating method, as described previously (Fukuda et al., 1996). Sections were incubated with a mouse anti-DARPP-32 antibody (sc-11365, 1:20,000 dilution, Santa Cruz Biotechnology) at 20°C for 7 d. Antibody binding was visualized with rhodamine red-conjugated donkey anti-mouse IgG (1:800, Jackson ImmunoResearch). Sections were mounted in Vectashield (Vector Laboratories), and the fluorescence of rhodamine red in the sections was observed using fluorescence microscopy (BZ-X710, Keyence). The long incubation period with the primary antibody was essential to improve the permeation of the antibody into the deep portions of the 50-μm-thick sections (Fukuda et al., 1998; Miyamoto et al., 2018).

Because the fiber bundle of white matter, which is composed of myelinated axons and oligodendrocytes, does not contain DARPP-32-positive MSNs or other types of DARPP-32-positive cells (Ouimet et al., 1998), the area of white matter was determined as DARPP-32-negative area in DARPP-32-immunostained striatal tissues. Using the Amira 6.5 software (Thermo Fisher Scientific), the section images were transformed to grayscale images and analyzed to determine the DARPP-32-positive and negative areas. The total and DARPP-32-positive areas in each subregion were determined in two coronal sections. The proportion of DARPP-32-positive areas in each subregion [$n = 3$; subregion (1), 87.75%; subregion (2-1), 82.19%; subregion (2-2), 88.67%; subregion (2-3), 88.01%; subregion (3), 83.18%; subregion (4), 75.72%; subregion (5), 88.50%] was used for protein normalization in each subregion.

Table 9. Statistical analysis for Figure 12

Set of data	Type of statistical analysis	Results of statistical analysis	
A, AIMs score (bottom left)			
Repeated measures two-way ANOVA for AIMs score on days 15 and 28			
Time effect	Two-way ANOVA	$F_{(5,215)} = 72.131$	$p < 0.001$
Day effect	Two-way ANOVA	$F_{(1,215)} = 36.646$	$p < 0.001$
Time-day interaction	Two-way ANOVA	$F_{(5,215)} = 20.363$	$p < 0.001$
20 min: day 15 vs day 28	Bonferroni *post hoc* test		$p < 0.001$
40 min: day 15 vs day 28	Bonferroni *post hoc* test		$p < 0.001$
60 min: day 15 vs day 28	Bonferroni *post hoc* test		$p < 0.001$
80 min: day 15 vs day 28	Bonferroni *post hoc* test		$p < 0.001$
A, AIMs score (bottom right)			
	t test	$t_{(36)} = 2.857$	$p = 0.0071$
B, P-Thr34 D32/D32			
Two-way ANOVA for subregion (1)			
SKF effect	Two-way ANOVA	$F_{(1,26)} = 18.56$	$p < 0.001$
6-OHDA effect	Two-way ANOVA	$F_{(1,26)} = 3.774$	$p = 0.0629$
SKF-6-OHDA interaction	Two-way ANOVA	$F_{(1,26)} = 2.627$	$p = 0.1171$
SKF: unlesioned side vs lesioned side	Bonferroni *post hoc* test		$p = 0.0095$
Two-way ANOVA for subregion (2-1)			
SKF effect	Two-way ANOVA	$F_{(1,26)} = 39.09$	$p < 0.001$
6-OHDA effect	Two-way ANOVA	$F_{(1,26)} = 9.687$	$p = 0.0045$
SKF-6-OHDA interaction	Two-way ANOVA	$F_{(1,26)} = 6.671$	$p = 0.0158$
SKF: unlesioned side vs lesioned side	Bonferroni *post hoc* test		$p < 0.001$
Two-way ANOVA for subregion (2-3)			
SKF effect	Two-way ANOVA	$F_{(1,26)} = 12.86$	$p = 0.0020$
6-OHDA effect	Two-way ANOVA	$F_{(1,26)} = 8.378$	$p = 0.0041$
SKF-6-OHDA interaction	Two-way ANOVA	$F_{(1,26)} = 6.027$	$p = 0.0524$
SKF: unlesioned side vs lesioned side	Bonferroni *post hoc* test		$p < 0.001$
Two-way ANOVA for subregion (3)			
SKF effect	Two-way ANOVA	$F_{(1,26)} = 15.19$	$p < 0.001$
6-OHDA effect	Two-way ANOVA	$F_{(1,26)} = 12.07$	$p = 0.0018$
SKF-6-OHDA interaction	Two-way ANOVA	$F_{(1,26)} = 5.824$	$p = 0.0232$
SKF: unlesioned side vs lesioned side	Bonferroni *post hoc* test		$p < 0.001$
Two-way ANOVA for subregion (4)			
SKF effect	Two-way ANOVA	$F_{(1,26)} = 20.82$	$p < 0.001$
6-OHDA effect	Two-way ANOVA	$F_{(1,26)} = 4.41$	$p = 0.0456$
SKF-6-OHDA interaction	Two-way ANOVA	$F_{(1,26)} = 2.443$	$p = 0.1302$
SKF: unlesioned side vs lesioned side	Bonferroni *post hoc* test		$p < 0.0077$
C, P-Ser845 GluA1/GluA1			
Two-way ANOVA for subregion (1)			
SKF effect	Two-way ANOVA	$F_{(1,26)} = 99.85$	$p < 0.001$
6-OHDA effect	Two-way ANOVA	$F_{(1,26)} = 26.99$	$p < 0.001$
SKF-6-OHDA interaction	Two-way ANOVA	$F_{(1,26)} = 25.25$	$p < 0.001$
SKF: unlesioned side vs lesioned side	Bonferroni *post hoc* test		$p < 0.001$
Two-way ANOVA for subregion (2-1)			
SKF effect	Two-way ANOVA	$F_{(1,26)} = 77.13$	$p < 0.001$
6-OHDA effect	Two-way ANOVA	$F_{(1,26)} = 11.51$	$p < 0.001$
SKF-6-OHDA interaction	Two-way ANOVA	$F_{(1,26)} = 9.612$	$p < 0.001$
SKF: unlesioned side vs lesioned side	Bonferroni *post hoc* test		$p < 0.001$
Two-way ANOVA for subregion (2-2)			
SKF effect	Two-way ANOVA	$F_{(1,26)} = 96.95$	$p < 0.001$
6-OHDA effect	Two-way ANOVA	$F_{(1,26)} = 7.709$	$p = 0.0101$
SKF-6-OHDA interaction	Two-way ANOVA	$F_{(1,26)} = 8.354$	$p = 0.0077$
SKF: unlesioned side vs lesioned side	Bonferroni *post hoc* test		$p < 0.001$

(*Table continues*.)

Table 9. Continued

Set of data	Type of statistical analysis	Results of statistical analysis	
Two-way ANOVA for subregion (2-3)			
SKF effect	Two-way ANOVA	$F_{(1,26)} = 181.4$	$p < 0.001$
6-OHDA effect	Two-way ANOVA	$F_{(1,26)} = 61.5$	$p < 0.001$
SKF-6-OHDA interaction	Two-way ANOVA	$F_{(1,26)} = 57.7$	$p < 0.001$
SKF: unlesioned side vs lesioned side	Bonferroni *post hoc* test		$p < 0.001$
Two-way ANOVA for subregion (3)			
SKF effect	Two-way ANOVA	$F_{(1,26)} = 50.38$	$p < 0.001$
6-OHDA effect	Two-way ANOVA	$F_{(1,26)} = 10.5$	$p = 0.0033$
SKF-6-OHDA interaction	Two-way ANOVA	$F_{(1,26)} = 9.212$	$p = 0.0054$
SKF: unlesioned side vs lesioned side	Bonferroni *post hoc* test		$p < 0.001$
Two-way ANOVA for subregion (4)			
SKF effect	Two-way ANOVA	$F_{(1,26)} = 43.54$	$p < 0.001$
6-OHDA effect	Two-way ANOVA	$F_{(1,26)} = 2.455$	$p = 0.1292$
SKF-6-OHDA interaction	Two-way ANOVA	$F_{(1,26)} = 5.093$	$p = 0.0326$
SKF: unlesioned side vs lesioned side	Bonferroni *post hoc* test		$p = 0.0055$
Two-way ANOVA for subregion (5)			
SKF effect	Two-way ANOVA	$F_{(1,26)} = 50.31$	$p < 0.001$
6-OHDA effect	Two-way ANOVA	$F_{(1,26)} = 5.654$	$p = 0.0251$
SKF-6-OHDA interaction	Two-way ANOVA	$F_{(1,26)} = 3.844$	$p = 0.0607$
SKF: unlesioned side vs lesioned side	Bonferroni *post hoc* test		$p = 0.0018$
D, P-Thr202/Tyr204 ERK2/ERK2			
Two-way ANOVA for subregion (1)			
SKF effect	Two-way ANOVA	$F_{(1,26)} = 75.53$	$p < 0.001$
6-OHDA effect	Two-way ANOVA	$F_{(1,26)} = 7.994$	$p = 0.0089$
SKF-6-OHDA interaction	Two-way ANOVA	$F_{(1,26)} = 12.65$	$p = 0.0015$
SKF: unlesioned side vs lesioned side	Bonferroni *post hoc* test		$p < 0.001$
Two-way ANOVA for subregion (2-1)			
SKF effect	Two-way ANOVA	$F_{(1,26)} = 46.62$	$p < 0.001$
6-OHDA effect	Two-way ANOVA	$F_{(1,26)} = 1.513$	$p = 0.2297$
SKF-6-OHDA interaction	Two-way ANOVA	$F_{(1,26)} = 3.755$	$p = 0.0636$
SKF: unlesioned side vs lesioned side	Bonferroni *post hoc* test		$p = 0.0217$
Two-way ANOVA for subregion (2-3)			
SKF effect	Two-way ANOVA	$F_{(1,26)} = 31.08$	$p < 0.001$
6-OHDA effect	Two-way ANOVA	$F_{(1,26)} = 1.367$	$p = 0.2529$
SKF-6-OHDA interaction	Two-way ANOVA	$F_{(1,26)} = 8.767$	$p = 0.0065$
SKF: unlesioned side vs lesioned side	Bonferroni *post hoc* test		$p = 0.0028$
Two-way ANOVA for subregion (3)			
SKF effect	Two-way ANOVA	$F_{(1,26)} = 47.14$	$p < 0.001$
6-OHDA effect	Two-way ANOVA	$F_{(1,26)} = 2.87$	$p = 0.1022$
SKF-6-OHDA interaction	Two-way ANOVA	$F_{(1,26)} = 3.895$	$p = 0.0591$
SKF: unlesioned side vs lesioned side	Bonferroni *post hoc* test		$p = 0.0076$
E, Ratio of increase in SKF treated			
P-Thr34 D32/D32	Linear regression	$y = 0.124\times - 1.193$ $p = 0.0158$ $r = 0.5375$	
P-Ser845 GluA1/GluA1	Linear regression	$y = 0.05033\times + 0.09139$ $p = 0.0399$ $r = 0.4287$	
P-Thr202/Tyr204 ERK2/ERK2	Linear regression	$y = 0.01781\times + 0.5953$ $p = 0.0143$ $r = 0.5485$	

Table 10. Statistical analysis for Figure 14

Set of data	Type of statistical analysis	Results of statistical analysis	
A, P-Thr34 D32/D32			
Two-way ANOVA for subregion (3)			
6-OHDA effect	Two-way ANOVA	$F_{(1,32)} = 12.97$	$p = 0.0011$
L-DOPA effect	Two-way ANOVA	$F_{(1,32)} = 3.143$	$p = 0.0858$
6-OHDA-L-DOPA interaction	Two-way ANOVA	$F_{(1,32)} = 6.714$	$p = 0.0143$
SKF: lesioned side vs lesioned side/L-DOPA	Bonferroni *post hoc* test		$p < 0.001$
B, P-Ser845 GluA1/GluA1			
Two-way ANOVA for subregion (1)			
6-OHDA effect	Two-way ANOVA	$F_{(1,32)} = 33.67$	$p < 0.001$
L-DOPA effect	Two-way ANOVA	$F_{(1,32)} = 5.994$	$p = 0.0200$
6-OHDA-L-DOPA interaction	Two-way ANOVA	$F_{(1,32)} = 1.057$	$p = 0.3115$
SKF: lesioned side vs lesioned side/L-DOPA	Bonferroni *post hoc* test		$p = 0.0391$
Two-way ANOVA for subregion (2-3)			
6-OHDA effect	Two-way ANOVA	$F_{(1,29)} = 78.45$	$p < 0.001$
L-DOPA effect	Two-way ANOVA	$F_{(1,29)} = 7.364$	$p = 0.0111$
6-OHDA-L-DOPA interaction	Two-way ANOVA	$F_{(1,29)} = 2.61$	$p = 0.1170$
SKF: lesioned side vs lesioned side/L-DOPA	Bonferroni *post hoc* test		$p = 0.0112$
Two-way ANOVA for subregion (3)			
6-OHDA effect	Two-way ANOVA	$F_{(1,32)} = 11.31$	$p = 0.0020$
L-DOPA effect	Two-way ANOVA	$F_{(1,32)} = 15.94$	$p < 0.001$
6-OHDA-L-DOPA interaction	Two-way ANOVA	$F_{(1,32)} = 4.663$	$p = 0.0384$
SKF: lesioned side vs lesioned side/L-DOPA	Bonferroni *post hoc* test		$p < 0.001$
Two-way ANOVA for subregion (5)			
6-OHDA effect	Two-way ANOVA	$F_{(1,31)} = 10.4$	$p = 0.0030$
L-DOPA effect	Two-way ANOVA	$F_{(1,31)} = 6.766$	$p = 0.0141$
6-OHDA-L-DOPA interaction	Two-way ANOVA	$F_{(1,31)} = 1.25$	$p = 0.2722$
SKF: lesioned side vs lesioned side/L-DOPA	Bonferroni *post hoc* test		$p = 0.0296$
C, P-Thr202/Tyr204 ERK2/ERK2			
Two-way ANOVA for subregion (3)			
6-OHDA effect	Two-way ANOVA	$F_{(1,32)} = 4.536$	$p = 0.0410$
L-DOPA effect	Two-way ANOVA	$F_{(1,32)} = 7.044$	$p = 0.0123$
6-OHDA-L-DOPA interaction	Two-way ANOVA	$F_{(1,32)} = 1.378$	$p = 0.2491$
SKF: lesioned side vs lesioned side/L-DOPA	Bonferroni *post hoc* test		$p = 0.0216$

Immunoprecipitations of Flag-tagged and Myc-tagged DARPP-32 in neostriatal slices from D1-DARPP-32-Flag/D2-DARPP-32-Myc mice

D1-DARPP-32-Flag/D2-DARPP-32-Myc transgenic mice express Flag-tagged and Myc-tagged DARPP-32 under the control of dopamine D1 and D2 receptor promoters, respectively (Bateup et al., 2008). In the striatum, Flag-tagged DARPP-32 was shown to be selectively expressed in D1 receptor-enriched striatonigral neurons, and Myc-tagged DARPP-32 selectively in D2 receptor-enriched striatopallidal neurons. Using antibodies against Flag and Myc tags, we selectively immunoprecipitated DARPP-32 from D1 receptor-expressing and D2 receptor-expressing neurons and analyzed the phosphorylation state of DARPP-32 in a neuronal subtype-specific manner in subregions (1), (2-3), and (3) as previously described (Nishi et al., 2008). In each subregion, 16–20 slices for control and papaverine treatment were collected from 8-10 mice and were used for the analysis of DARPP-32 phosphorylation.

Unilateral 6-hydroxydopamine (6-OHDA) lesion of dopaminergic neurons at the medial forebrain bundle (MFB)

Mice were anesthetized with pentobarbital sodium (40 mg/kg, i.p.) and mounted in a stereotaxic frame equipped with a mouse adaptor. 6-OHDA was dissolved in saline containing 0.05% ascorbic acid at a concentration of 3 mg of free-base 6-OHDA/ml. To protect noradrenergic neurons, mice were pretreated with desipramine (20 mg/kg, i.p.) 30 min before the injection of 6-OHDA. 6-OHDA was injected at a dose of 3 μg (1–1.5 μl) into the right MFB (AP = −1.2 mm anterior, ML = −1.2 mm lateral from the bregma, and DV = 4.8 mm ventral from the skull's surface). Two weeks after 6-OHDA injection, behavioral tests and slice experiments were performed. Lesioning of dopaminergic neurons in the striatum was evaluated by determining the protein levels of TH. Only animals with the TH level reduction of >80% in all subregions were included in the analyses.

Pole test

The pole test was performed to evaluate bradykinesia induced by 6-OHDA lesion as previously described (Tanimura et al., 2019). The mice were placed head-upward on the top of a vertical, wooden pole (50 cm in height, 1 cm in diameter), and the time until the mice descended to the floor was recorded. After 1 d of training (three trials for each session), the time was measured before and after the 6-OHDA injection (five trials for each session). Each testing trial lasted for a maximum of 120 s. When the mouse was not able to turn downward and/or dropped from the pole, the descendent time was taken as 120 s.

Cylinder test

The cylinder test was performed to evaluate forelimb akinesia induced by 6-OHDA lesion as previously described (Schallert and Tillerson, 2000; Santini et al., 2007). The mice were placed in individual glass cylinders (20 cm in height and 15 cm in diameter). The number of wall contacts with the right and the left forelimbs was counted for 5 min before and after the 6-OHDA injection. To discriminate between accidental touches and meaningful physiological movements, only wall contacts where the animal supported its body weight on the paw with extended

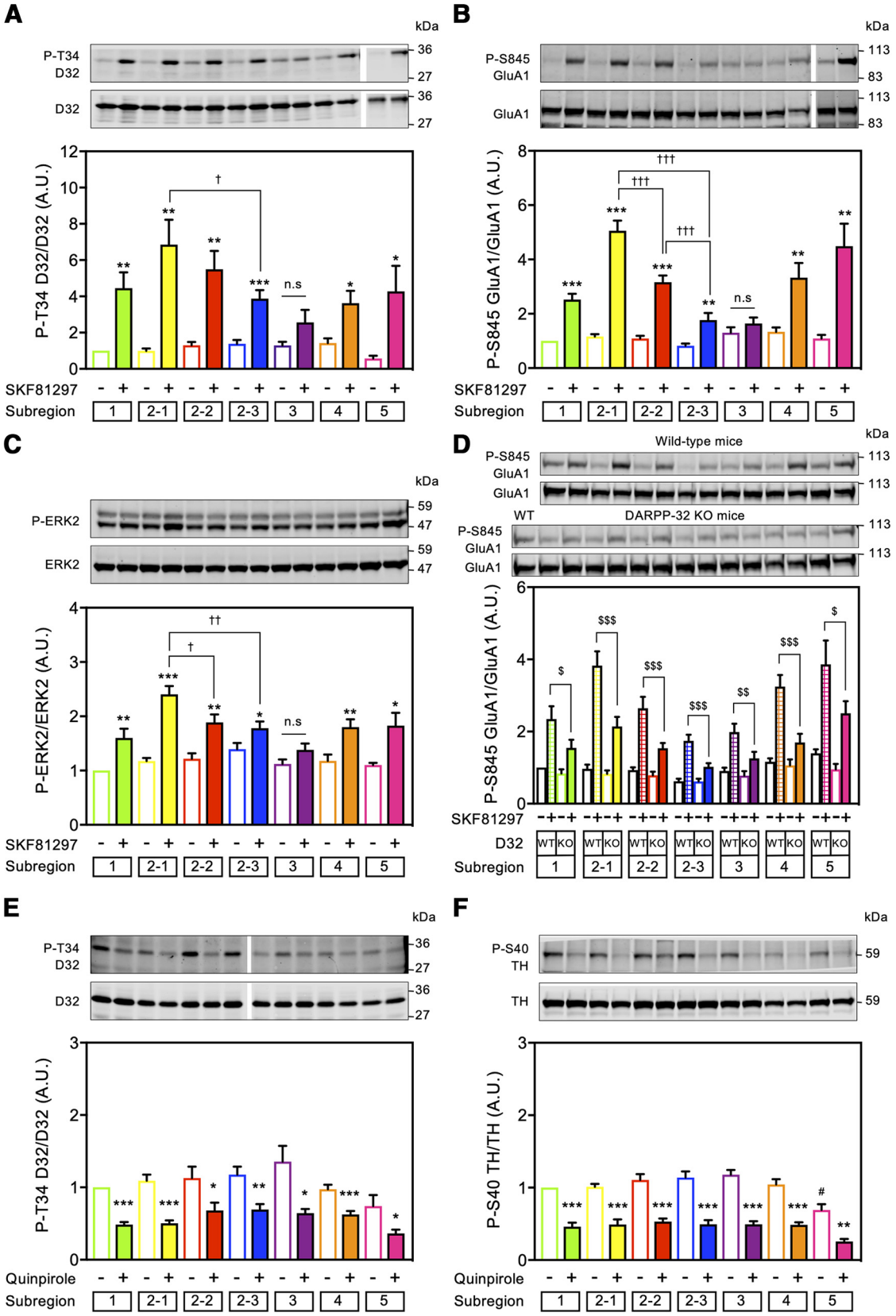

Figure 2. Effects of dopamine D1 and D2 receptor activation on protein phosphorylation in the seven subregions of the striatum. The effects of the D1 receptor agonist, SKF81297 (1 μM for 10 min; ***A–D***), and a D2 receptor agonist, quinpirole (1 μM for 10 min; ***E***, ***F***), were examined in the seven subregions of striatal slices prepared from C57BL/6N mice (***A–C***, ***E***, ***F***) and DARPP-32 knock-out (KO) mice (***D***). The phosphorylation of DARPP-32 (D32) at Thr34 (***A***, ***E***), GluA1 at Ser845 (***B***, ***D***), ERK2 at Thr202/Tyr204 (***C***), and TH at Ser40 (***F***) were determined by Western blotting using phosphorylation state-specific antibodies. Typical immunoblots for detection of phospho-proteins and total proteins are shown with quantitation. Phospho-proteins were normalized to total proteins, and then data were normalized to values obtained with SKF81297-untreated slices in subregion (1). Total proteins in each subregion, which were corrected for the proportions of DARPP-32-positive areas (Fig. 3), are shown in Figure 4*A–D*. Data of DARPP-32 KO mice were normalized to values obtained with SKF81297-untreated slices in subregion (1) from wild-type

digits were counted. The use of the impaired forelimb (left) was expressed as a percentage of the total number of supporting wall contacts.

Asymmetrical abnormal involuntary movements (AIMs)

6-OHDA-lesioned mice were treated with L-DOPA (6 mg/kg, i.p.) and benserazide (12 mg/kg, i.p.) once daily for 14 d. AIMs were assessed after the last injection of L-DOPA (Lundblad et al., 2004, 2005); 20 min after L-DOPA administration, the mice were placed in separate cages, and individual dyskinetic behaviors were assessed for 1 min (monitoring period) every 20 min over a period of 120 min. Purposeless movements, clearly distinguished from natural stereotyped behaviors (i.e., grooming, sniffing, rearing, and gnawing), were classified into four different subtypes: locomotive AIMs (tight contralateral turns), axial AIMs (contralateral dystonic posture of the neck and upper body toward the side contralateral to the lesion), limb AIMs (jerky and fluttering movements of the limb contralateral to the side of the lesion), and orolingual AIMs (vacuous jaw movements and tongue protrusions). Each subtype was scored on a severity scale from 0 to 4: 0, absent; 1, occasional; 2, frequent; 3, continuous; 4, continuous and not interruptible by external stimuli. Mice were used for slice experiments within 20–24 h after AIMs assessment.

Statistical analysis

The data are displayed as mean ± SEM. The significance of differences within each group was determined with one-way ANOVA followed by Bonferroni *post hoc* test or Newman–Keuls *post hoc* test. When two groups were compared, paired or unpaired Student's *t* test or two-way ANOVA followed by Bonferroni *post hoc* test was used. The analyses were performed using GraphPad Prism 7.0 (GraphPad Software).Repeated measures two-way ANOVA followed by Bonferroni *post hoc* test were used to compare the experimental groups. The analysis was performed using SigmaPlot 14 (Systat Software Inc). $p < 0.05$ was considered to be significant. Details of the statistical analyses are listed in Table 1-Table 10.

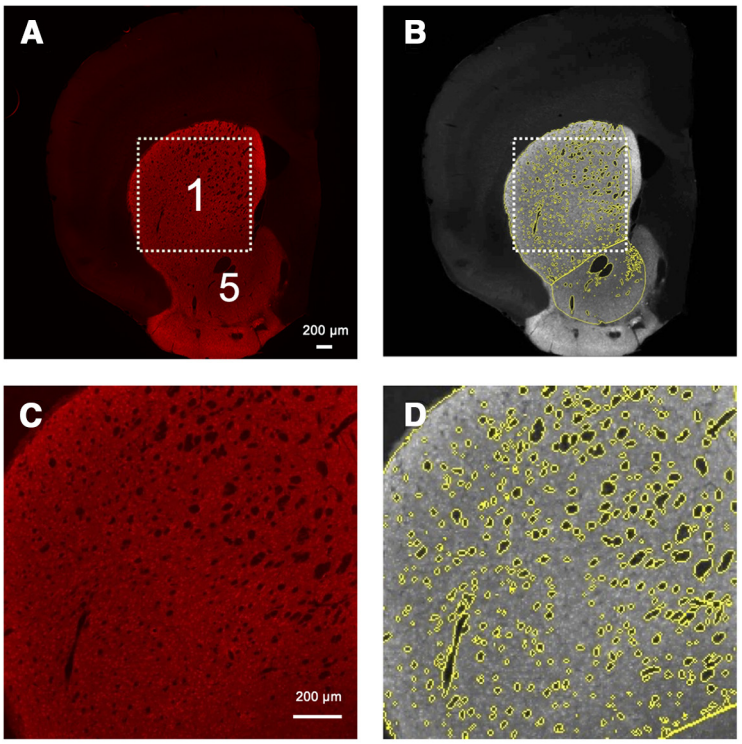

E

DARPP-32 positive area

Subregion	mean± SE (%)	Correction value
(1)	87.75 ± 2.22	1.14
(5)	88.50 ± 0.69	1.13
(2-1)	82.19 ± 2.54	1.22
(2-2)	88.67 ± 1.34	1.13
(2-3)	88.01 ± 0.80	1.14
(3)	83.18 ± 0.28	1.20
(4)	75.72 ± 5.22	1.32

Figure 3. Analysis of DARPP-32 positive area. Immunoreactivity for DARPP-32 in subregions (1) and (5). The enlarged area in ***C***, ***D*** is indicated by the white dotted line (***A***, ***B***). The fluorescent intensity of DARPP-32-immunostaining was transformed to the gray level using Amira 6.5 software (Thermo Fisher Scientific; ***B***, ***D***). The DARPP-32-negative areas were clearly distinguished and corresponded to the yellow contours (***D***). The table shows the proportions of DARPP-32-positive areas and the correction values used for normalization of protein levels in the seven subregions of the striatum (***E***). Data represent mean ± SEM for three experiments.

Results

Dopamine D1 and D2 receptor signaling in the seven subregions of the striatum

To investigate dopamine signaling in the seven subregions of the striatum, striatal slices from the seven subregions were prepared and the effects of a D1 receptor agonist, SKF81297, or a D2 receptor agonist, quinpirole, on the phosphorylation of PKA substrates (DARPP-32 at Thr34, GluA1 at Ser845, and/or TH at Ser40) and/or a downstream substrate of PKA signaling (ERK2 at Thr202/Tyr204) were examined (Fig. 2). After normalization with the proportion of DARPP-32-positive area in each subregion of the striatum (see Materials and Methods and Fig. 3), the expression of DARPP-32, GluA1, and TH was low in subregion (4) of the C part along the rostrocaudal axis (Fig. 4*A*,*B*,*D*). The expression of ERK2 was higher in subregion (2–1) than in subregion (1) of the dorsal striatum (Fig. 4*C*). Along the mediolateral axis, the expression of ERK2 was low in subregion (2-3) of the DL-IR part compared with subregion (2-1) of the M-IR part. Subregion (5) of the NAc showed a different expression profile: low in DARPP-32 and TH and high in ERK2 compared with subregion (1) of the dorsal striatum.

The basal phosphorylation levels of DARPP-32, GluA1, and ERK2 were similar among the subregions (Fig. 2*A*–*C*). Treatment of slices with SKF81297 (1 μM) increased the

←

(WT) mice (***D***). The effects of the A_{2A} receptor agonist on the phosphorylation of DARPP-32 are shown in Figure 5. Data represent mean ± SEM for 6–11 experiments (***A–C***, ***E***, ***F***) and 9–10 experiments (***D***); $*p < 0.05$, $**p < 0.01$, $***p < 0.001$ compared with untreated slices in each subregion; Student's *t* test (***A–C***, ***E***, ***F***); $\dagger p < 0.05$, $\dagger\dagger p < 0.01$, $\dagger\dagger\dagger p < 0.001$ compared with SKF81297-treated slices among subregions (2-1), (2-2), and (2-3); two-way ANOVA followed by Bonferroni *post hoc* test (***A–C***); $\$p < 0.05$, $\$\$p < 0.01$, $\$\$\$p < 0.001$ compared with SKF-treated slices in WT mice in each subregion; two-way ANOVA followed by Bonferroni *post hoc* test (***D***); $\#p < 0.05$ compared with untreated slices in other subregions; one-way ANOVA followed by Bonferroni *post hoc* test (***F***). n.s., not significant. Details of the statistical analyses are listed in Table 1.

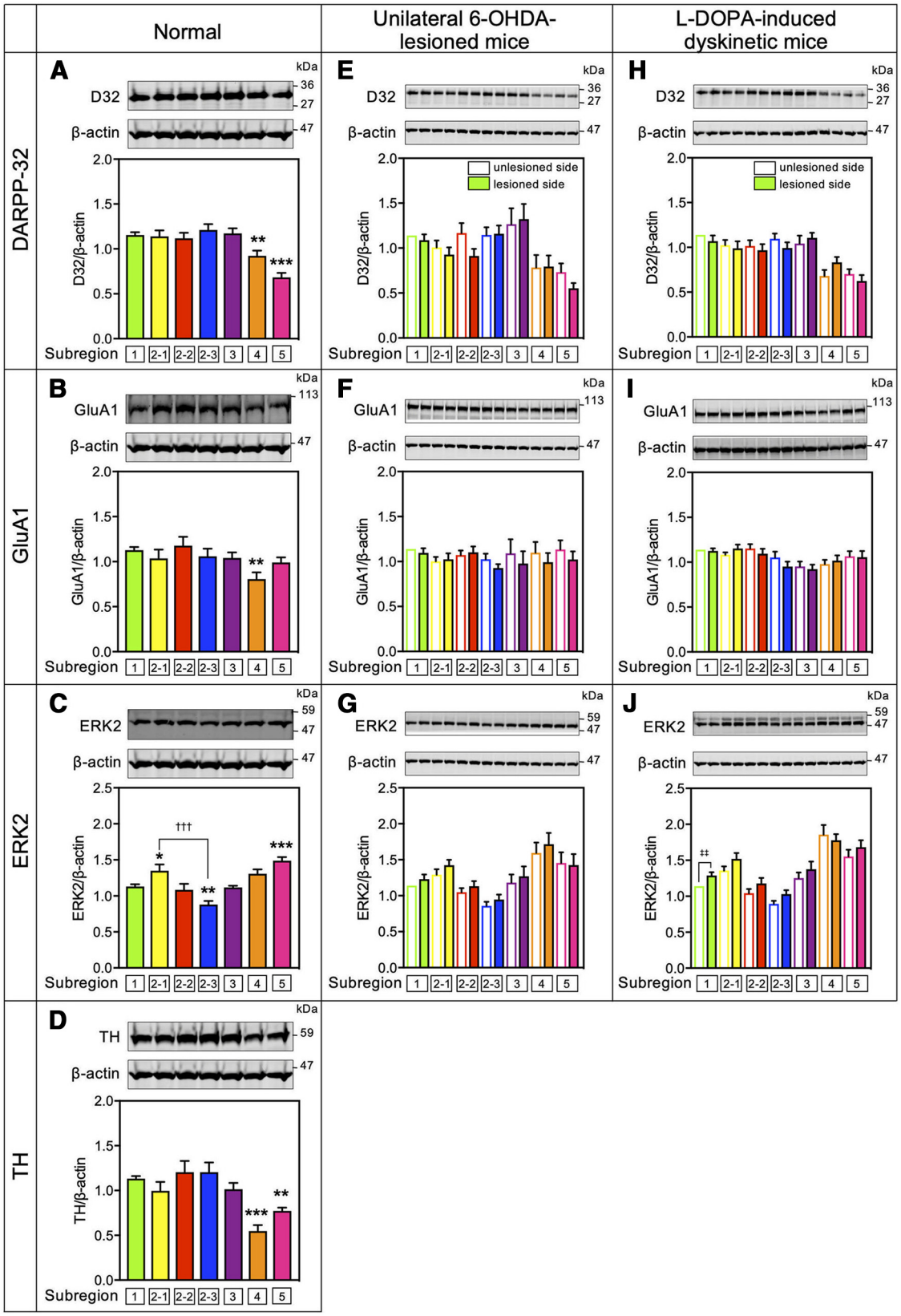

Figure 4. Expression levels of DARPP-32, GluA1, ERK2, and TH in the striatum. The protein expression levels of DARPP-32 (D32; ***A***, ***E***, ***H***), GluA1 (***B***, ***F***, ***I***), ERK2 (***C***, ***G***, ***J***), and TH (***D***) were determined in the seven subregions of the striatum. The samples (25 μg) were loaded onto the gel. Typical immunoblots are shown with quantitation. The expression levels were normalized to β-actin and values obtained with slices from subregion (1) (***A–D***) or from the unlesioned side of subregion (1) (***E–J***). After the normalization, data were corrected for the proportions of DARPP-32-positive areas. Data represent mean ± SEM for 6–10 (***A–D***), 12–14 (***E–G***), or 13 (***H–J***) experiments; $^{*}p < 0.05$, $^{**}p < 0.01$, $^{***}p < 0.001$ compared with slices in subregion (1); one-way ANOVA followed by Bonferroni *post hoc* test; $^{\dagger\dagger\dagger}p < 0.001$ compared with slices in subregion (2-1) for analysis along the mediolateral axis; one-way ANOVA followed by Bonferroni *post hoc* test; $^{\ddagger\ddagger}p < 0.01$ compared with slices from the unlesioned side; Student's *t* test. Details of the statistical analyses are listed in Table 2.

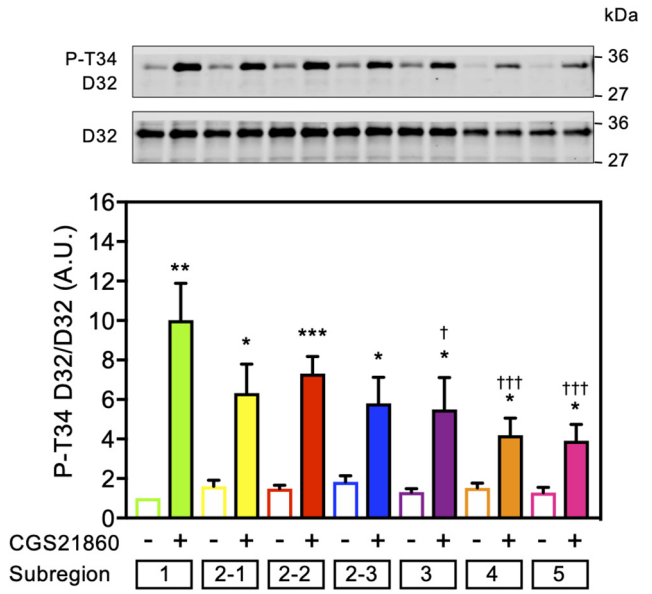

Figure 5. Effects of CGS21860 on the phosphorylation of DARPP-32 in the seven subregions of the striatum. Striatal slices of the seven subregions were incubated with the adenosine A_{2A} receptor agonist, CGS21680 (5 μM for 10 min). Slices were pretreated with adenosine deaminase (30 μg/ml for 60 min) to reduce the tissue content of adenosine and the basal phosphorylation levels of DARPP-32 (D32) at Thr34. The phosphorylation of DARPP-32 at Thr34 was determined by Western blotting. Typical immunoblots for detection of phospho-proteins and total proteins are shown with quantitation. Data were normalized to values obtained with CGS21680-untreated slices in subregion (1). Data represent mean ± SEM for six to seven experiments; $^{*}p < 0.05$, $^{**}p < 0.01$, $^{***}p < 0.001$ compared with untreated slices in each subregion; Student's *t* test; †$p < 0.05$, †††$p < 0.001$ compared with CGS21860-treated slices in subregion (1); two-way ANOVA followed by Bonferroni *post hoc* test. Details of the statistical analyses are listed in Table 3.

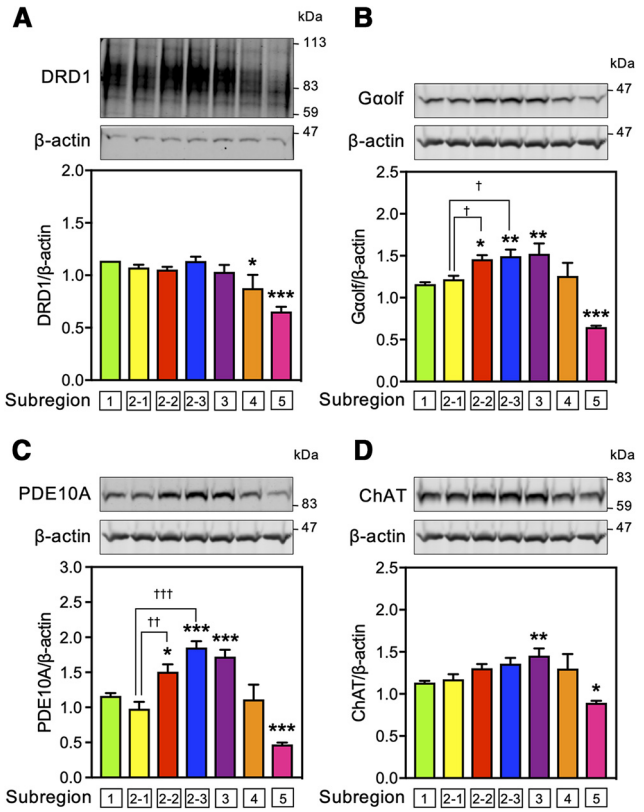

Figure 6. Expression levels of proteins involved in dopamine signaling in the seven subregions of the striatum. The protein expression levels of DRD1 (***A***), Gαolf (***B***), PDE10A (***C***), and ChAT (***D***) were determined in striatal slices from seven subregions. The samples [3 μg (DRD1) or 25 μg (Gαolf, PDE10A, and ChAT)] were loaded onto the gel. Typical immunoblots are shown with quantitation. The expression levels were normalized to β-actin and values obtained with slices in subregion (1). After the normalization, data were corrected for the proportions of DARPP-32-positive areas. Data represent mean ± SEM for 6–10 experiments; $^{*}p < 0.05$, $^{**}p < 0.01$, $^{***}p < 0.001$ compared with slices in subregion (1); one-way ANOVA followed by Bonferroni *post hoc* test; †$p < 0.05$, ††$p < 0.01$, †††$p < 0.001$ compared with slices in subregion (2-1) for analysis along the mediolateral axis; one-way ANOVA followed by Bonferroni *post hoc* test. Details of the statistical analyses are listed in Table 4.

phosphorylation of DARPP-32, GluA1, and ERK2 in almost all subregions, but not in subregion (3) of the IC part (Fig. 2*A–C*). Along the mediolateral axis, the effects of SKF81297 on the phosphorylation of DARPP-32, GluA1, and ERK2 were high in subregion (2-1) of the M-IR and low in subregion (2-3) of the DL-IR part.

To investigate the role of DARPP-32 in the seven subregions, the effects of SKF81297 on GluA1 phosphorylation were examined in striatal slices from DARPP-32 knock-out mice. In wild-type mice, the effect of SKF81297 was low in subregion (3) along the rostrocaudal axis and low in subregion (2-3) along the mediolateral axis, as observed in C57BL/6N mice. The effects of SKF81297 were reduced in all subregions of DARPP-32 knock-out mice (Fig. 2*D*), suggesting that the contribution of DARPP-32-mediated PP-1 inhibition to GluA1 phosphorylation is similar among the seven subregions.

Next, we examined the effects of a D2 receptor agonist, quinpirole (1 μM), on the phosphorylation of DARPP-32 at Thr34 and TH at Ser40 in slices from the seven subregions (Fig. 2*E*,*F*). The basal phosphorylation levels of TH at dopaminergic terminals were low in the subregion (5) of the NAc compared with the other subregions. Treatment of slices with quinpirole (1 μM) decreased the phosphorylation of DARPP-32 and TH in all subregions to a similar extent. To evaluate the activation of cAMP/PKA signaling in D2-type MSNs (Ferré et al., 2008), the effects of the adenosine A_{2A} receptor agonist, CGS21860, on DARPP-32 phosphorylation were examined (Fig. 5). Treatment with CGS21680 (5 μM) increased DARPP-32 phosphorylation in all subregions with the highest effect observed in subregions (1). As differential regulation of D1 receptor signaling in D1-type MSNs among subregions of the striatum was apparent compared with that of D2 receptor signaling in D2-type MSNs, we further characterized D1 receptor signaling in D1-type MSNs in the seven subregions.

Expression levels of proteins involved in D1 receptor signaling in the seven subregions of the striatum

To investigate the mechanisms of differential regulation, the expression levels of proteins involved in D1 receptor/cAMP/PKA signaling were determined in the seven subregions of the striatum. The expression levels of DRD1 were similar in subregions (1)–(3) of the dorsal striatum, but slightly lower in subregion (4) (Fig. 6*A*). In subregions (2-3) and/or (3), where the activity of D1 receptor signaling was low, PDE10A and ChAT were expressed at high levels (Fig. 6*C*,*D*). Since PDE10A and ChAT subsequently counteract D1 receptor signaling, the high expression of PDE10A and ChAT likely contributes to the low activity of D1 receptor signaling. Gαolf was expressed at high levels in subregions (2-3) and (3) (Fig. 6*B*), which may serve as a compensatory mechanism of low D1 receptor signaling. In subregion (5) of the NAc, the expression levels of DRD1, Gαolf, PDE10A, and ChAT were lower than those in the subregions of the dorsal striatum.

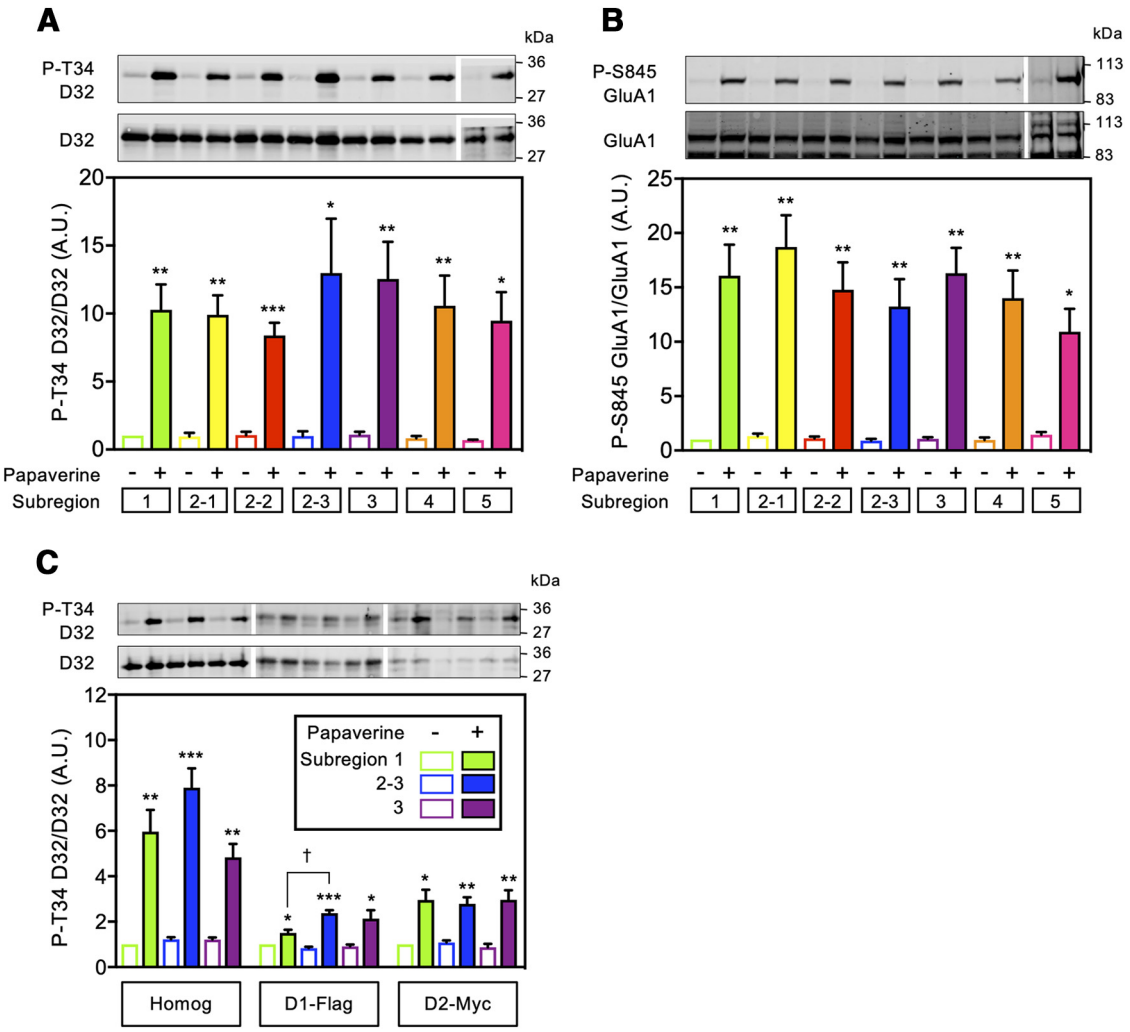

Figure 7. Effects of papaverine on the phosphorylation of DARPP-32 and GluA1 in the seven subregions of the striatum. ***A***, ***B***, Striatal slices of the seven subregions were incubated with a PDE10A inhibitor, papaverine (10 μM for 60 min). ***C***, Striatal slices of subregions (1), (2-3), and (3) prepared from D1-DARPP-32-Flag/D2-DARPP-32-Myc mice were incubated with papaverine (10 μM for 60 min), and Flag-tagged DARPP-32, expressed in D1-type MSNs, and Myc-tagged DARPP-32, expressed in D2-type MSNs, were immunoprecipitated. The figure shows data from total striatal homogenate (Homog), Flag-tagged DARPP-32 in D1-type MSNs (D1-Flag), and Myc-tagged DARPP-32 in D2-type MSNs (D2-Myc). The phosphorylation of DARPP-32 (D32) at Thr34 (***A***, ***C***) and GluA1 at Ser845 (***B***) were determined by Western blotting. Typical immunoblots for detection of phospho-proteins and total proteins are shown with quantitation. Data were normalized to values obtained with untreated slices in subregion (1). Data represent mean ± SEM for four to six experiments (***A***, ***B***) or five to six experiments (***C***); $^{*}p < 0.05$, $^{**}p < 0.01$, $^{***}p < 0.001$ compared with untreated slices in each subregion; Student's *t* test; †$p < 0.05$ compared with papaverine-treated slices in subregion (1); two-way ANOVA followed by Bonferroni *post hoc* test. Details of the statistical analyses are listed in Table 5.

Role of PDE10A in low D1 receptor signaling

To examine whether PDE10A contributes to the downregulation of D1 receptor signaling in subregions (2-3) and (3), the effects of a PDE10A inhibitor, papaverine, on the phosphorylation of DARPP-32 and GluA1 were examined in the seven subregions of the striatum. The treatment of slices with papaverine (10 μM) induced a large increase in the phosphorylation of DARPP-32 and GluA1 in all subregions (Fig. 7*A*,*B*). Next, we examined the effects of papaverine (10 μM) on DARPP-32 phosphorylation in D1-type and D2-type MSNs in subregions (2-3) and (3) using striatal slices from D1-DARPP-32-Flag/D2-DARPP-32-Myc transgenic mice (Bateup et al., 2008; Nishi et al., 2008). The inhibition of PDE10A by papaverine induced the phosphorylation of Flag-tagged and Myc-tagged DARPP-32 in D1-type and D2-type MSNs, respectively, in subregions (1), (2-3), and (3), and the phosphorylation levels of Flag-tagged DARPP-32 in D1-type MSNs were higher in subregion (2-3) than in subregion (1) (Fig. 7*C*). In agreement with a previous report (Nishi et al., 2008), the effects of papaverine in D1-type MSNs were smaller than those in D2-type MSNs. These results suggest that PDE10A-mediated degradation of cAMP may be involved in the downregulation of D1 receptor signaling in subregions (2-3) and (3).

Roles of muscarinic receptors in low D1 receptor signaling

Acetylcholine released from cholinergic interneurons has been shown to activate M4 receptors in D1-type MSNs and counteract D1 receptor signaling (Onali and Olianas, 2002; Nair et al., 2019). The expression of ChAT was high in subregion (3) (Fig. 6*D*), where the activity of D1 receptor signaling was low. Therefore, we examined whether acetylcholine/muscarinic receptor signaling contributes to the downregulation of D1 receptor signaling in subregions (2-3) and (3). For this purpose, the effects of SKF81297 on the phosphorylation of DARPP-32 and GluA1 were examined in the presence of a muscarinic receptor antagonist, atropine, or an M4-selective muscarinic toxin, MT3. Pretreatment of striatal slices with atropine (1 μM) or MT3 (100

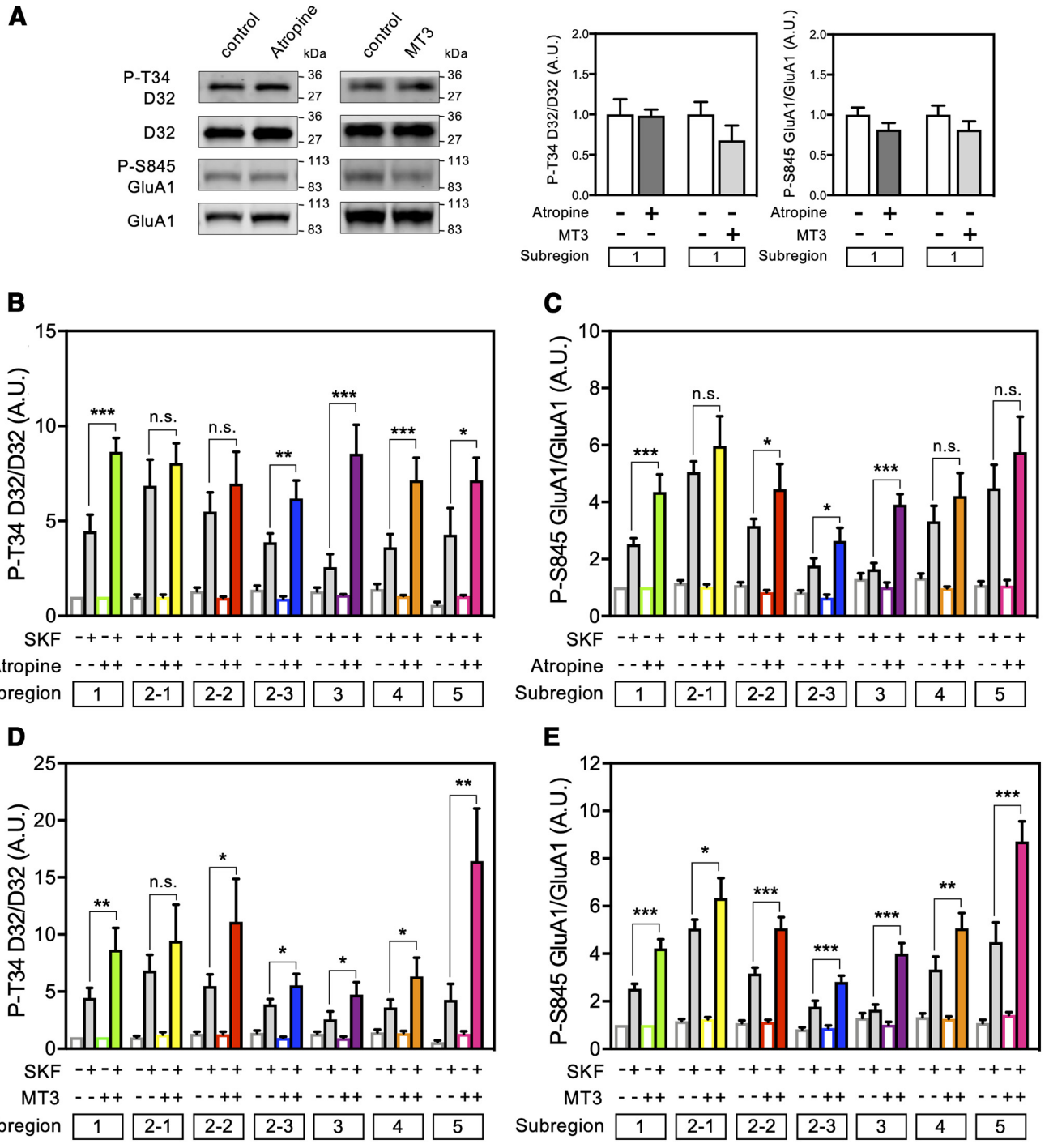

Figure 8. Effects of atropine or MT3 on SKF81297-induced phosphorylation of DARPP-32 and GluA1 in the seven subregions of the striatum. Striatal slices of the seven subregions were pre-incubated with a non-selective muscarinic receptor antagonist, atropine (1 μM for 10 min; ***A–C***), or an M4 receptor-selective muscarinic toxin, MT3 (100 nM for 60 min; ***A***, ***D***, ***E***), and then incubated with SKF81297 (1 μM for 10 min) in the presence of atropine or MT3. The phosphorylation levels of DARPP-32 at Thr34 (***A***, ***B***, ***D***) and GluA1 at Ser845 (***A***, ***C***, ***E***) were determined by Western blotting. Treatment with atropine or MT3 alone did not affect the basal phosphorylation levels of DARPP-32 or GluA1 in subregion (1) (***A***). Data in the presence of atropine or MT3 were normalized to values obtained with atropine or MT3 alone in subregion (1) (***B–E***). Data in the absence of atropine and MT3 were reproduced from Figure 2*A*,*B* for comparison (open and filled gray bars). Data represent mean ± SEM for four to seven experiments (***A***) and five to eight experiments (***B–E***); *$p < 0.05$, **$p < 0.01$, ***$p < 0.001$ compared with SKF-treated slices without atropine or MT3 pretreatment in each subregion; one-way ANOVA followed by Newman–Keuls *post hoc* test. n.s., not significant. Details of the statistical analyses are listed in Table 6.

nM) did not affect the basal phosphorylation levels of DARPP-32 or GluA1 in subregion (1) (Fig. 8*A*) or other subregions (Fig. 8*B–E*). Pretreatment with atropine or MT3 enhanced the SKF81297-induced increase in the phosphorylation of DARPP-32 and GluA1 in subregions (2-3) and (3) with low D1 receptor signaling and some other subregions (Fig. 8*B–E*). These results suggest that muscarinic M_4 receptors play a critical role in the downregulation of D1 receptor signaling in subregions with low D1 receptor signaling.

D1 receptor signaling in 6-OHDA-lesioned hemiparkinsonian mice

To evaluate D1 receptor signaling under pathophysiological conditions of Parkinson's disease, 6-OHDA was injected into the

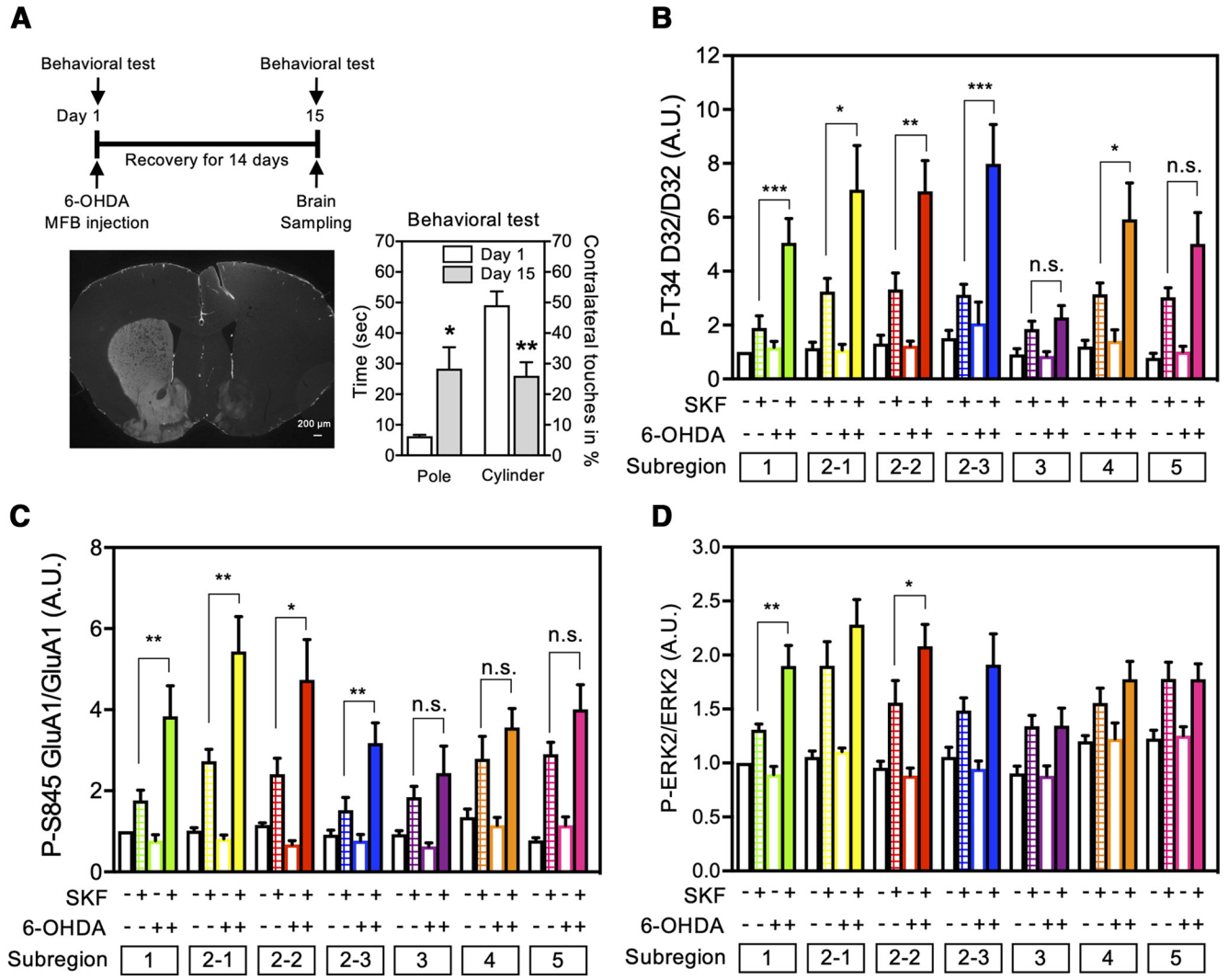

Figure 9. Effects of SKF81297 on the phosphorylation of DARPP-32, GluA1, and ERK2 in the seven subregions of the striatum in unilateral 6-OHDA-lesioned mice. ***A***, Experimental design for unilateral 6-OHDA-lesioned mice (top). The mice received a unilateral injection of 6-OHDA into the right MFB. Immunoreactivity of TH in unlesioned and lesioned sides of the striatum (bottom left). Fluorescent signal of TH was converted to grayscale. In behavioral tests, total descent time in the pole test and left forelimb use in the cylinder test were determined before (day 1) and after unilateral 6-OHDA lesion (day 15; bottom right). Data represent mean ± SEM for 11 experiments; $^{*}p < 0.05$, $^{**}p < 0.01$ compared with data before 6-OHDA injection (day 1); Student's *t* test. ***B–D***, Striatal slices of the seven subregions were incubated with SKF81297 (1 μM for 10 min). The phosphorylation of DARPP-32 at Thr34 (***B***), GluA1 at Ser845 (***C***), and ERK2 at Thr202/Tyr204 (***D***) were determined by Western blotting. Data of slices untreated or treated with SKF81297 were obtained separately and thereafter combined (Fig. 10). Unilateral 6-OHDA lesion did not affect the basal phosphorylation of DARPP-32, GluA1, or ERK in slices from the unlesioned side of subregion (1) compared with slices from subregion (1) of control mice (data not shown), and therefore data of slices untreated and treated with SKF81297 were normalized to values obtained with SKF81297-untreated slices from the unlesioned side of subregion (1) in 6-OHDA-lesioned mice and from subregion (1) in control mice, respectively. The expression of proteins in each subregion are shown in Figures 4*E–G*, 11*A–D*. Data represent mean ± SEM for six to eight experiments; $^{*}p < 0.05$, $^{**}p < 0.01$, $^{***}p < 0.001$ compared with SKF-treated slices from the unlesioned side in each subregion; two-way ANOVA followed by Bonferroni *post hoc* test. n.s., not significant. Details of the statistical analyses are listed in Table 7.

right MFB (Fig. 9*A*). 6-OHDA lesion decreased TH levels by >80% from levels of the unlesioned side in all subregions (Fig. 10). Unilateral 6-OHDA-lesioned mice showed behavioral deficits in the pole and cylinder tests on day 15 (Fig. 9*A*). The protein expression levels of DARPP-32, GluA1, or ERK2 (Fig. 4*E–G*) or the basal phosphorylation of DARPP-32, GluA1, or ERK2 (Fig. 9*B–D*) were not affected by 6-OHDA lesion. 6-OHDA lesion enhanced the effects of SKF81297 on the phosphorylation of DARPP-32 and GluA1 in almost all subregions including subregion (2-3), but not in subregion (3) or subregion (5) (Fig. 9*B*,*C*). Enhancement of ERK2 phosphorylation was observed only in subregions (1) and (2–2) (Fig. 9*D*). Despite the enhancement of D1 receptor signaling, the protein expression levels of DRD1, Gαolf, PDE10A, and ChAT were similar before and after 6-OHDA lesion, except for small changes in subregions (1) and/or (2-1) (Fig. 11*A–D*). These results demonstrate that, in 6-OHDA-lesioned hemi-parkinsonian mice, dopaminergic denervation upregulates DRD1 signaling in almost all subregions, including subregion (2–3), but DRD1 signaling remains downregulated in subregion (3).

D1 receptor signaling in a mouse model of LID

Sensitized D1 receptor signaling has been shown to play a critical role in the development of LID (Feyder et al., 2011). Therefore, we examined D1 receptor signaling in the seven subregions of the striatum in a mouse model of LID. In unilateral 6-OHDA-lesioned mice, administration of L-DOPA plus benserazide once daily for 14 d (Fig. 12*A*) induced an increase in AIMs scores on day 28 (Fig. 12*A*), suggesting the development of LID (Lundblad et al., 2004, 2005). Striatal slices of the seven subregions were

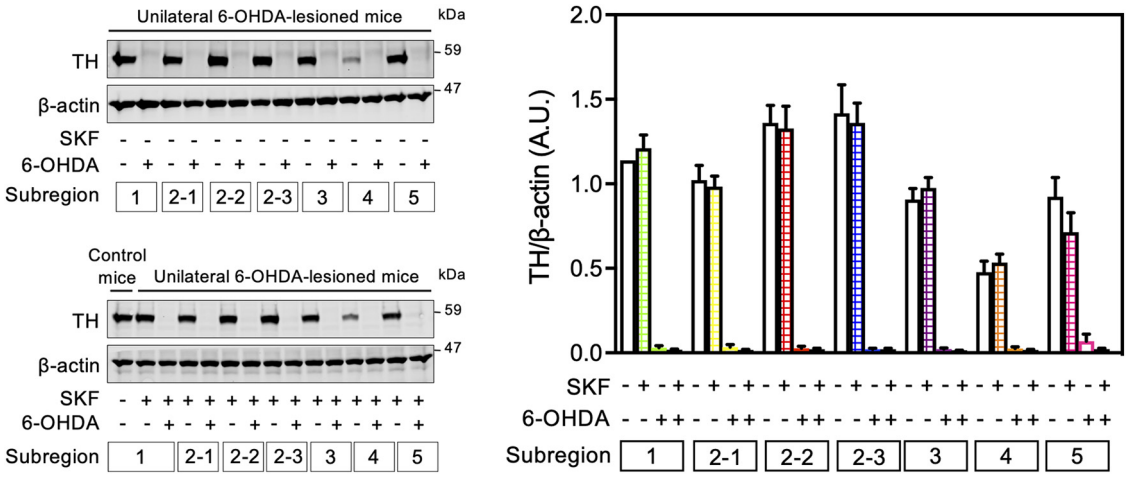

Figure 10. Effects of 6-OHDA lesion on TH expression levels in the seven subregions of the striatum. TH levels of unlesioned and 6-OHDA-lesioned sides were determined in striatal slices of the seven subregions, which were obtained separately in slices untreated (upper panel) or treated (lower panel) with SKF81297. The samples (25 μg) were loaded onto the gel. Typical immunoblots are shown with quantitation. In slices untreated with SKF81297 (upper panel), the expression levels were normalized to β-actin and values obtained with SKF81297-untreated slices from the unlesioned side of subregion (1). As unilateral 6-OHDA lesion did not affect the expression levels of TH in slices from the unlesioned side of subregion (1) compared with slices from subregion (1) of control mice (data not shown), the expression levels of TH in SKF81297-treated slices (lower panel) were normalized to β-actin and values obtained from SKF8129-untreated slices from subregion (1) of control mice. After the normalization, data were corrected for the proportions of DARPP-32-positive areas. Data represent mean ± SEM for six to eight experiments.

prepared from LID mice, in which TH levels of the 6-OHDA-lesioned side decreased by >80% compared with those of the unlesioned side (Fig. 13). In LID mice, the protein expression levels (Fig. 4*H–J*) and the basal phosphorylation levels (Fig. 12*B–D*) of DARPP-32, GluA1, and ERK2 were similar between the unlesioned and 6-OHDA-lesioned sides in almost all subregions. SKF81297-induced phosphorylation of DARPP-32, GluA1, and ERK2 in the 6-OHDA-lesioned side was higher than that in the unlesioned side in most of subregions (Fig. 12*B–D*).

To evaluate whether D1 receptor signaling is enhanced in LID mice, the effects of SKF81297 on the phosphorylation of DARPP-32, GluA1, and ERK2 were compared among four conditions: unlesioned and lesioned sides of unilateral 6-OHDA-lesioned (Fig. 9*B–D*) and LID (Fig. 12*B–D*) mice. The comparison of DARPP-32, GluA1, and ERK2 phosphorylation clearly showed that SKF81297-stimulated D1 receptor signaling in subregion (3) was enhanced in the 6-OHDA-lesioned side of LID mice (Fig. 14*A–C*). These results demonstrate that DRD1 signaling in subregion (3) is suppressed under normal conditions and not enhanced by 6-OHDA lesion, but enhanced in LID.

The protein expression levels of DRD1 were not affected by 6-OHDA lesion or 6-OHDA lesion plus L-DOPA treatment (Fig. 11*A*,*E*). However, in immunoblots of DRD1, a downward shift of DRD1 bands induced by 6-OHDA lesion plus L-DOPA treatment was observed in subregions (1)–(4) of the dorsal striatum, although not observed in subregion (5) of the NAc (Fig. 11*E*), suggesting that L-DOPA treatment induces the posttranslational modification of DRD1 in the 6-OHDA-lesioned side of LID mice. Analyses of proteins involved in D1 receptor signaling revealed an increase in Gαolf in subregions (3) of the 6-OHDA-lesioned side as previously reported (Alcacer et al., 2012; Fig. 11*F*).

We further examined whether there was a correlation between the severity of AIMs and the enhancement of SKF81297-induced phosphorylation of DARPP-32, GluA1, and ERK2 by 6-OHDA lesion in LID mice. In line with a previous report (Santini et al., 2007), simple linear regression analyses revealed a significant correlation between AIMs score and the ratio of the 6-OHDA-lesioned side to the unlesioned side for SKF81297-induced phosphorylation of DARPP-32, GluA1, and ERK2 only in subregion (3) of LID mice (Fig. 12*E*).

Discussion

In the present study, we demonstrated that D1 receptor signaling in D1-type MSNs was differentially regulated in seven subregions of the striatum. Low D1 receptor signaling was detected in two subregions: (1) the DL-IR part (2-3) and (2) the IC part (3). Low D1 receptor signaling was maintained through the high cAMP degradation by PDE10A and the high cholinergic tone via M4 receptors. In an animal model of Parkinson's disease, D1 receptor signaling was upregulated in almost all subregions, including DL-IR (2-3), but not in IC (3). When LID was developed, an increase in D1 receptor signaling in IC (3), which correlated with the severity of LID, was observed, suggesting that the upregulation of D1 receptor signaling in IC (3) was involved in LID. Thus, the subregion-specific regulation of D1 receptor signaling is important for maintaining the function of the striatum, and subregion-specific derangement of D1 receptor signaling may be responsible for motor symptoms of Parkinson's disease and LID.

Striatal subregions with low D1 receptor signaling

We identified striatal subregions with low D1 receptor signaling: DL-IR (2-3) and IC (3). However, low D1 receptor signaling was not mediated through the low expression of D1 receptors. The expression of D1 receptors is enriched in the striosome (Crittenden and Graybiel, 2011; Brimblecombe and Cragg, 2017). The proportion of D1-type MSNs that constitute the striosomes gradually decreases along the mediolateral direction: 70% in substance P-positive striosomes, 40% in substance P-deficient striosomes, and 30% in striosome-free space (Miyamoto et al., 2018). However, clear differences in the densities of D1-type MSNs along the mediolateral and ventrodorsal axes were not detected (Ren et al., 2017), probably because striosomes occupy only 10–15% of striatal volume (Crittenden and Graybiel, 2011; Brimblecombe and Cragg, 2017). An autoradiographic study revealed a decrease in D1 receptor binding sites in the

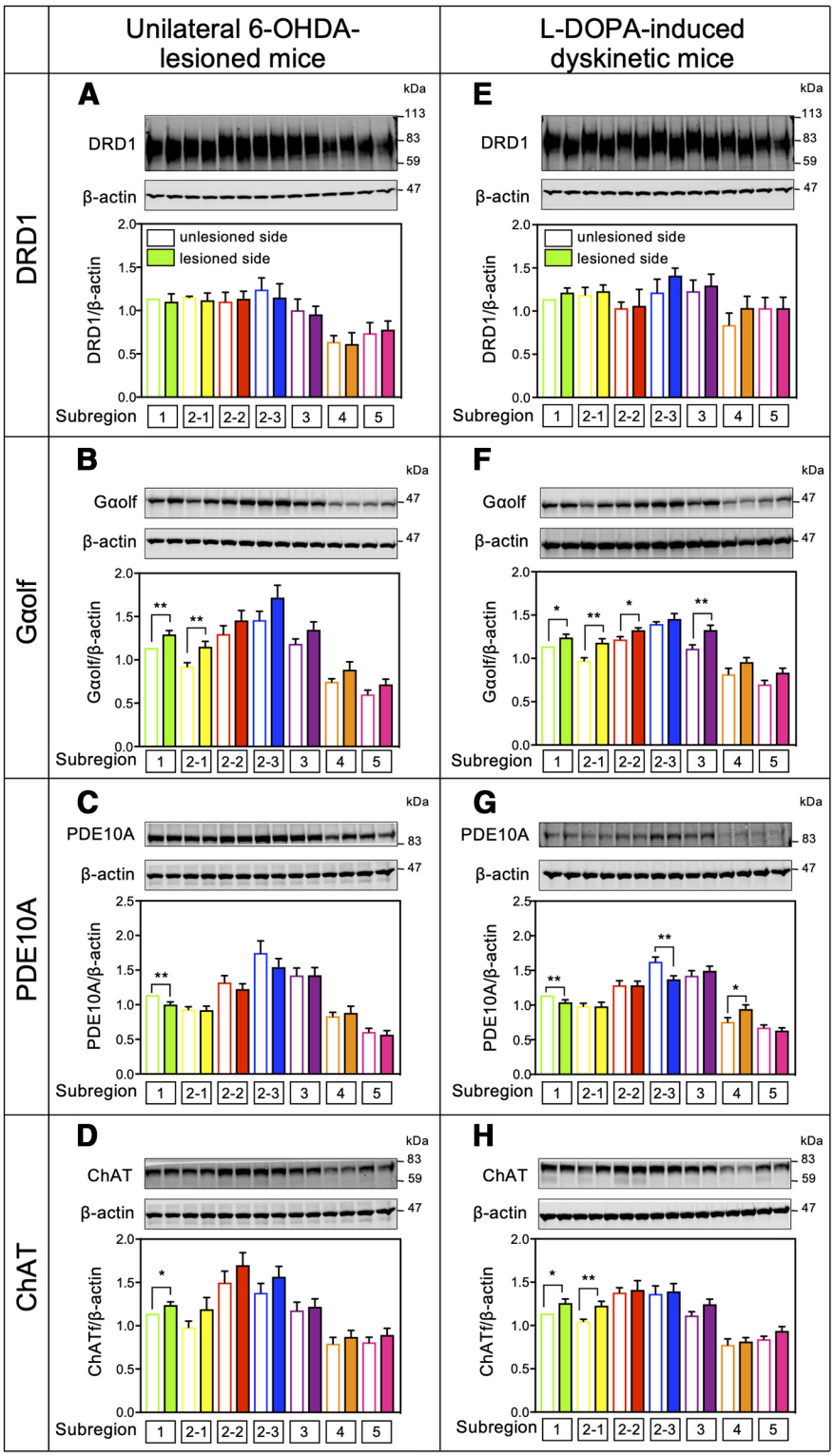

Figure 11. Expression levels of proteins involved in dopamine signaling in animal models of 6-OHDA-induced hemi-parkinsonism and LID. The protein expression levels of DRD1 (***A***, ***E***), Gαolf (***B***, ***F***), PDE10A (***C***, ***G***), and ChAT (***D***, ***H***) were determined in the seven subregions of the striatum. The samples [25 μg (Gαolf, PDE10A, ChAT) or 3 μg (DRD1)] were loaded onto the gel. Typical immunoblots are shown with quantitation. The expression levels were normalized to β-actin and values obtained with slices from the unlesioned side of subregion (1). After the normalization, data were corrected for the proportions of DARPP-32-positive areas. Data were collected from both the SKF-untreated and SKF-treated slices in each subregion. Data represent mean ± SEM for three experiments (***A***), 12–14 experiments (***B–D***), five experiments (***E***), and 13 experiments (***F–H***); $*p < 0.05$, $**p < 0.01$ compared with unlesioned side; Student's *t* test. Details of the statistical analyses are listed in Table 8.

rostrocaudal direction in the medial portion of the rat striatum (Boyson et al., 1986), which is consistent with our findings showing low expression of D1 receptors in the C part of the striatum.

The density of D1 receptors and the expression pattern of D1 receptors at the soma, dendrites and axon terminals in D1-type MSNs are not well characterized in the striosome and matrix (Levey et al., 1993; Yung et al., 1995; Wei et al., 2017). Interestingly, D1 receptors have been reported to modulate D1-type MSNs oppositely in the striosome and matrix (Prager et al., 2020). Activation of D1 receptors in D1-type MSNs prolongs the generation of long-lasting synaptically evoked up-states in the matrix, but opposes it in the striosome. The opposite effects are induced by altered modulation of glutamatergic input by D1 receptors, but not by altered activation of D1 receptors. The differences in modulatory machineries of D1 receptor signaling between the striosome and matrix may contribute to the subregion-specificity of D1 receptor signaling.

The activity of the D1 receptor/cAMP/PKA signaling pathway is regulated by PDE. In the striatum, PDE10A is highly expressed and plays a major role in cAMP degradation (Nishi et al., 2008). The high expression of PDE10A in DL-IR (2-3) and IC (3) contributes to the maintenance of low D1 receptor signaling. It has been shown that the action of PDE10A is predominant in D2-type MSNs compared with D1-type MSNs (Nishi et al., 2008; Threlfell et al., 2009; Polito et al., 2015). However, in D1-type MSNs, a high PDE10A function to maintain low D1 receptor signaling was identified in DL-IR (2-3) and IC (3). Our results also demonstrated that cholinergic tone is high in IC (3), because of the high expression levels of ChAT. As subsequent activation of M4 receptors in D1-type MSNs counteracts D1 receptor signaling (Onali and Olianas, 2002; Kuroiwa et al., 2012; Nair et al., 2019), the high cholinergic tone seems to play a critical role in maintaining low D1 receptor signaling.

D1 receptor signaling in the NAc

The ability of D1 receptors to mediate PKA-dependent phosphorylation of DARPP-32 and GluA1 in the NAc and dorsal striatum were not distinguishable despite receiving distinct dopaminergic innervation from the VTA and SNpc, respectively, and the different expression profiles of dopamine signaling molecules (TH, D1 receptors, Gαolf, DARPP-32,

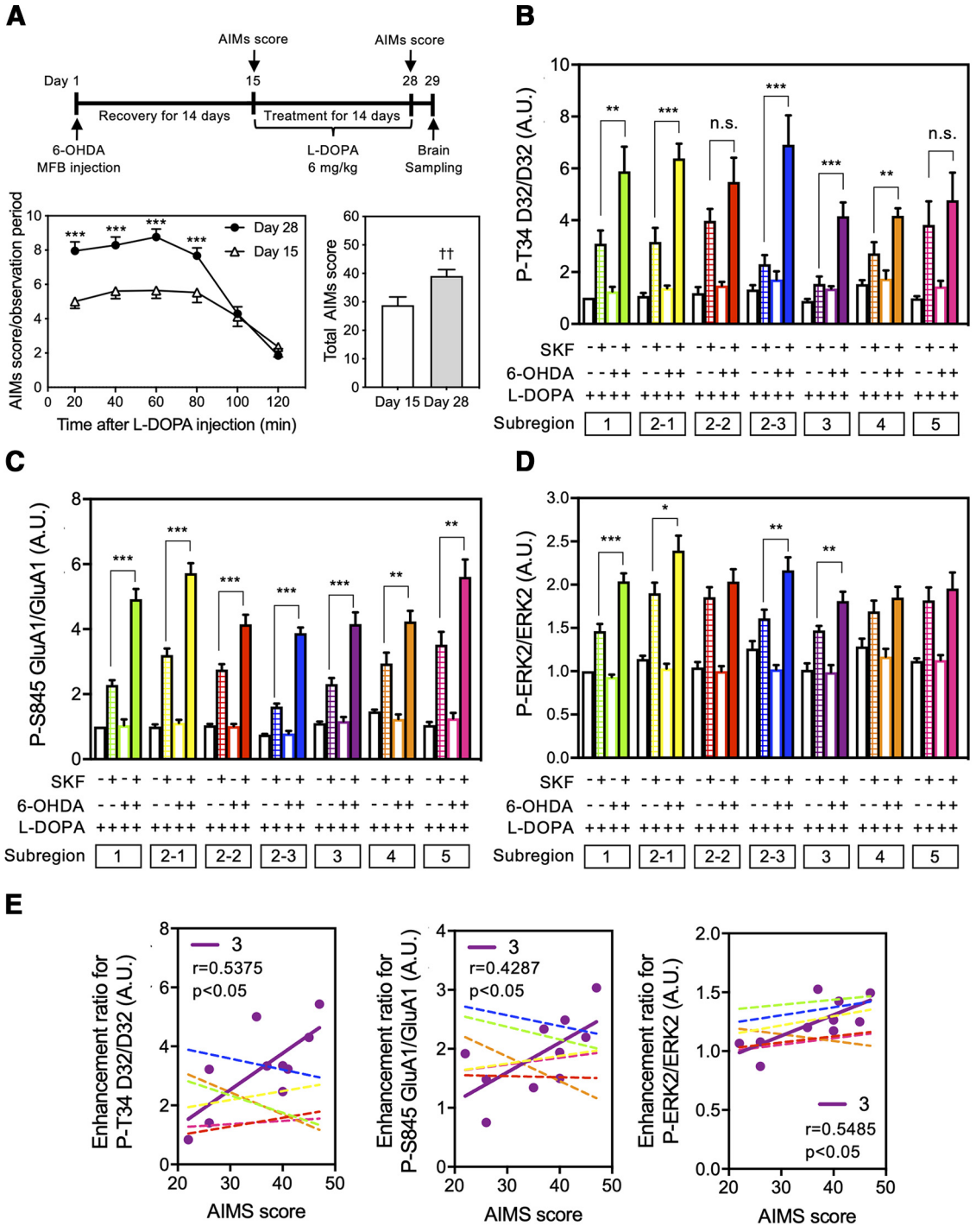

Figure 12. Effects of SKF81297 on the phosphorylation of DARPP-32, GluA1, ERK2 in the seven subregions of the striatum in a mouse model of LID. ***A***, An experimental design for a mouse model of LID (top). Unilateral 6-OHDA-lesioned mice were treated with L-DOPA (6 mg/kg, i.p.) plus benserazide (12 mg/kg, i.p.) for 14 d from day 15 to day 28. AIM scale scoring was performed on days 15 and 28. Total axial, limb, orolingual, and locomotive AIMs were scored every 20 min over a period of 120 min (bottom left). Total AIMs score was calculated as the sum of scores during all observation periods (bottom right). Data represent mean ± SEM for 17–21 experiments; $^{***}p < 0.001$ compared with day 15; repeated measures two-way ANOVA followed by Bonferroni *post hoc* test (bottom left); $^{††}p < 0.01$ compared with day 15; Student's *t* test (bottom right). ***B–D***, Striatal slices of the seven subregions were prepared from LID mice, and were incubated with SKF81297 (1 μM for 10 min). The phosphorylation of DARPP-32 at Thr34, GluA1 at Ser845, and ERK2 at Thr202/Tyr204 were determined by Western blotting. Data of slices untreated or treated with SKF81297 were obtained separately and thereafter combined (Fig. 13). Unilateral 6-OHDA lesion and L-DOPA treatment did not affect the basal phosphorylation of DARPP-32, GluA1, or ERK2 in slices from the unlesioned side of subregion (1) compared with slices from subregion (1) of control mice (data not shown), and therefore data of slices untreated and treated with SKF81297 were normalized to values obtained with SKF81297-untreated slices from unlesioned side of subregion (1) in 6-OHDA-lesioned/L-DOPA-treated mice and from subregion (1) in control mice, respectively. The expression of proteins in each subregion are shown in Figures 4*H–J*,11*E–H*. Comparison of data for SKF81297-stimulated D1 receptor signaling between animal models of 6-OHDA-induced hemi-parkinsonism and LID are shown in Figure 14. Data represent mean ± SEM for 5–10 experiments; $^{*}p < 0.05$, $^{**}p < 0.01$, $^{***}p < 0.001$ compared with SKF81297-treated slices from the unlesioned side in each subregion; two-way ANOVA followed by Bonferroni *post hoc* test. n.s., not significant. ***E***, Simple linear regression analyses between AIMs score on day 28 and the enhancement of SKF81297-induced phosphorylation of DARPP-32, GluA1, and ERK2 by 6-OHDA lesion (ratio of the 6-OHDA-lesioned side to the 6-OHDA-unlesioned side for SKF81297-induced phosphorylation) in LID mice. The color of each line corresponds to the colors of the seven subregions in ***B–D***. Details of the statistical analyses are listed in Table 9.

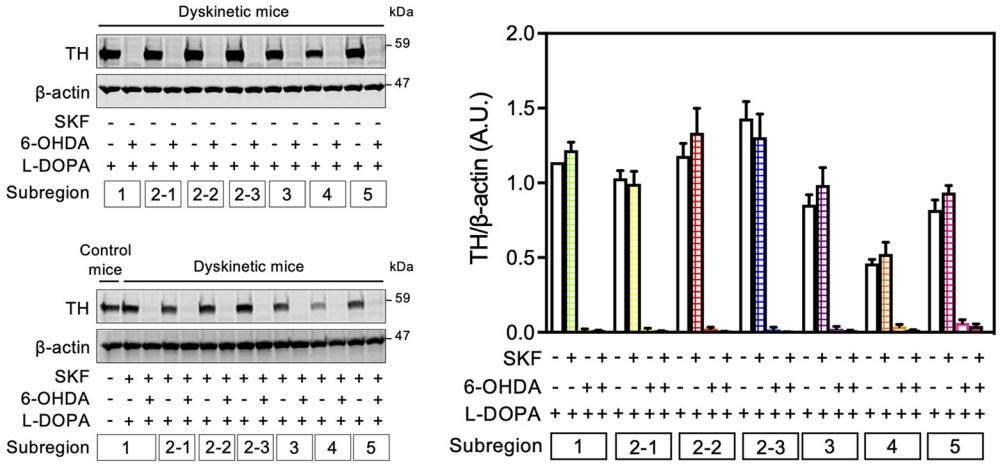

Figure 13. TH expression levels in a mouse model of LID. TH levels of the unlesioned and 6-OHDA-lesioned sides in LID mice were determined in striatal slices of the seven subregions, which were obtained separately in slices untreated (upper panel) or treated (lower panel) with SKF81297. The samples (25 μg) were loaded onto the gel. Typical immunoblots are shown with quantitation. In slices untreated with SKF81297 (upper panel), the expression levels were normalized to β-actin and values obtained with SKF81297-untreated slices from the unlesioned side of subregion (1). As unilateral 6-OHDA lesion and L-DOPA treatment did not affect the expression levels of TH in slices from unlesioned side of subregion (1) compared with slices from subregion (1) of control mice (data not shown), the expression levels of TH in slices treated with SKF81297 (lower panel) were normalized to β-actin and values obtained with SKF81297-untreated slices from subregion (1) of control mice. After the normalization, data were corrected for the proportions of DARPP-32-positive areas. Data represent mean ± SEM for six to eight experiments.

PDE10A, and ChAT). In addition, dorsal to ventral gradients in the amounts of dopamine release, the kinetics of dopamine reuptake, and the density of dopaminergic innervation have been reported (Jones et al., 1995; Cragg et al., 2002; Pacelli et al., 2015; Salgado and Kaplitt, 2015; Marcott et al., 2018). We speculate that the balance of components that promote and counteract D1 receptor signaling is controlled to elicit optimal responses in the NAc, and therefore the NAc-specific features of D1 receptor signaling may not be identified.

Subregion-specific upregulation of D1 receptor signaling in animal models of hemi-parkinsonism and LID

It is well established that dopamine depletion in the striatum induces D1 receptor sensitization in D1-type MSNs, resulting in the upregulation of cAMP/PKA and ERK signaling (Gerfen et al., 2002; Santini et al., 2007; Spigolon and Fisone, 2018). In this study, dopamine depletion induced upregulation of D1 receptor/cAMP/PKA signaling in most subregions including DL-IR (2-3) with low D1 receptor signaling, but not in IC (3). Upregulation of D1 receptor signaling may be attributable to the increased expression of Gαolf (Alcacer et al., 2012) in R (1) and M-IR (2-1). Furthermore, the fact that upregulation of ERK phosphorylation is limited in R (1) and C-IR (2-2) suggests no tight relationship between activities of D1 receptor/cAMP/PKA and D1 receptor/ERK signaling. If we consider that ERK activation has been evaluated in the rostral and IR parts of the striatum in animal models of Parkinson's disease, the upregulation of subregion-specific ERK phosphorylation is in line with previous findings (Santini et al., 2007; Alcacer et al., 2012). Taken together, the upregulation of D1 receptor signaling in response to dopamine depletion is subregion-specific, using various signaling molecules.

In LID, following the original priming event of D1 receptor signaling to dopamine depletion, the chronic administration of L-DOPA induces secondary molecular alterations of the D1 receptor signaling machinery, which is associated with the development of LID (Spigolon and Fisone, 2018). D1 receptor signaling becomes more responsive to acute L-DOPA treatment, resulting in the enhancement of cAMP/PKA/DARPP-32 and ERK signaling (Gerfen et al., 2002; Santini et al., 2007). In this study, the enhancement of D1 receptor/cAMP/PKA signaling and D1 receptor/ERK signaling over dopamine-depleted conditions in LID mice is limited to IC (3). Furthermore, the enhancement of DARPP-32 and ERK phosphorylation in IC (3) correlated with the severity of LID. Identification of molecular mechanisms for D1 receptor sensitization in IC (3) is required to understand the pathophysiology of LID.

Functional role of D1 receptor signaling in IC (3) of the striatum in motor function

Low D1 receptor signaling is a feature of IC (3) as well as DL-IR (2-3) of the striatum, which receives projections from the sensorimotor cortex (Hintiryan et al., 2016; Hunnicutt et al., 2016). Although we did not evaluate this under *in vivo* conditions, low D1 receptor signaling in IC (3) and DL-IR (2-3) may be required to maintain adequate excitability of D1-type MSNs, when activated by glutamatergic projections from the sensorimotor cortex. In a mouse model of 6-OHDA-lesioned hemi-parkinsonism, the suppression of D1 receptor signaling in DL-IR (2-3) was removed, possibly to compensate for dopamine depletion. When LID was developed, the suppression of D1 receptor signaling in IC (3) was removed, resulting in aberrant activation of D1 receptor signaling and presumably hyperexcitability of D1-type MSNs in IC (3) (Feyder et al., 2011). These findings suggest that D1 receptor signaling in IC (3) needs to be regulated at optimal activity levels to maintain motor function under normal and pathophysiological conditions.

Girasole et al. (2018) demonstrated that a subset of D1-type MSNs in the striatal region projected from the sensorimotor cortex is responsible for LID. In the study, the subset of D1-type MSNs, activated by L-DOPA in LID mice, in the area corresponding to DL-IR (2-3) and IC (3) was optogenetically activated

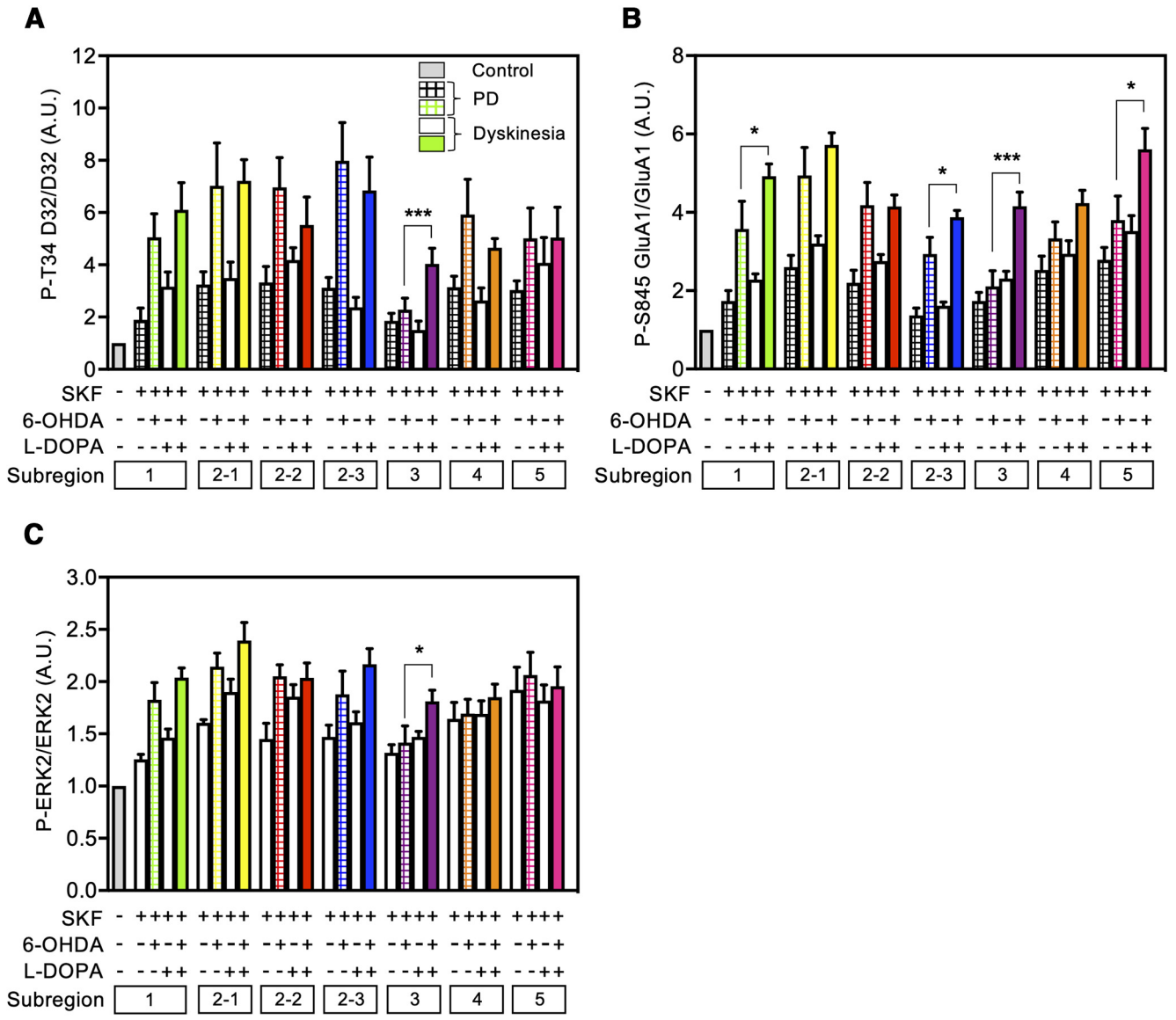

Figure 14. Comparison of SKF81297-stimulated D1 receptor signaling between animal models of 6-OHDA-induced hemi-parkinsonism and LID. SKF81297-stimulated phosphorylation of DARPP-32 at Thr34 (***A***), GluA1 at Ser845 (***B***), and ERK2 at Thr202/Tyr204 (***C***) was compared between the unilateral 6-OHDA-lesioned mice (using data in Fig. 9*B–D*) and LID mice (using data in Fig. 12*B–D*). Data were normalized to values obtained with SKF81297-untreated slices from subregion (1) of control mice; $*p < 0.05$, $***p < 0.001$ compared with SKF-treated slices from 6-OHDA-lesioned side in unilateral 6-OHDA-lesioned mice in each subregion; two-way ANOVA followed by Bonferroni *post hoc* test. Details of the statistical analyses are listed in Table 10.

using the targeted recombination in active populations (TRAP) system. The increased expression of thyrotropin-releasing hormone selectively in DL-IR (2-3) and IC (3) in LID rats also indicates the importance of these subregions (Cantuti-Castelvetri et al., 2010). Our findings suggest that a subset of D1-type MSNs in IC (3) plays a critical role in LID. However, D1-type MSNs causally linked to LID have been investigated mainly in DL-IR (2-3) in previous functional and behavioral studies (Perez et al., 2017; Ryan et al., 2018). Future studies are required to clarify the role of D1 receptor signaling and D1-type MSNs in IC (3) in LID.

In conclusion, we identified striatal subregions of DL-IR (2-3) and IC (3) with low D1 receptor signaling, where MSNs receive glutamatergic projections from sensorimotor cortex. Furthermore, in a mouse model of LID, aberrant activation of D1 receptor signaling in IC (3) was associated with LID. Identification of the molecular mechanisms by which D1 receptor signaling in IC (3) is activated in LID will facilitate the development of novel therapeutics for LID.

References

Alcacer C, Santini E, Valjent E, Gaven F, Girault JA, Hervé D (2012) Gα(olf) mutation allows parsing the role of cAMP-dependent and extracellular signal-regulated kinase-dependent signaling in L-3,4-dihydroxyphenylalanine-induced dyskinesia. J Neurosci 32:5900–5910.

Alexander GE, Crutcher MD (1990) Functional architecture of basal ganglia circuits: neural substrates of parallel processing. Trends Neurosci 13:266–271.

Bateup HS, Svenningsson P, Kuroiwa M, Gong S, Nishi A, Heintz N, Greengard P (2008) Cell type-specific regulation of DARPP-32 phosphorylation by psychostimulant and antipsychotic drugs. Nat Neurosci 11:932–939.

Bertran-Gonzalez J, Hervé D, Girault JA, Valjent E (2010) What is the degree of segregation between striatonigral and striatopallidal projections? Front Neuroanat 4:136.

Boyson SJ, McGonigle P, Molinoff PB (1986) Quantitative autoradiographic localization of the D1 and D2 subtypes of dopamine receptors in rat brain. J Neurosci 6:3177–3188.

Brimblecombe KR, Cragg SJ (2017) The striosome and matrix compartments of the striatum: a path through the labyrinth from neurochemistry toward function. ACS Chem Neurosci 8:235–242.

Bromberg-Martin ES, Matsumoto M, Hikosaka O (2010) Dopamine in motivational control: rewarding, aversive, and alerting. Neuron 68:815–834.

Cantuti-Castelvetri I, Hernandez LF, Keller-McGandy CE, Kett LR, Landy A, Hollingsworth ZR, Saka E, Crittenden JR, Nillni EA, Young AB, Standaert DG, Graybiel AM (2010) Levodopa-induced dyskinesia is associated with increased thyrotropin releasing hormone in the dorsal striatum of hemi-parkinsonian rats. PLoS One 5:e13861.

Cragg SJ, Hille CJ, Greenfield SA (2002) Functional domains in dorsal striatum of the nonhuman primate are defined by the dynamic behavior of dopamine. J Neurosci 22:5705–5712.

Crittenden JR, Graybiel AM (2011) Basal Ganglia disorders associated with imbalances in the striatal striosome and matrix compartments. Front Neuroanat 5:59.

Ferré S, Quiroz C, Woods A, Cunha R, Popoli P, Ciruela F, Lluis C, Franco R, Azdad K, Schiffmann S (2008) An update on adenosine A2A-dopamine D2 receptor interactions: implications for the function of G protein-coupled receptors. Curr Pharm Des 14:1468–1474.

Feyder M, Bonito-Oliva A, Fisone G (2011) L-DOPA-induced dyskinesia and abnormal signaling in striatal medium spiny neurons: focus on dopamine D1 receptor-mediated transmission. Front Behav Neurosci 5:71.

Fienberg AA, Hiroi N, Mermelstein PG, Song W, Snyder GL, Nishi A, Cheramy A, O'Callaghan JP, Miller DB, Cole DG, Corbett R, Haile CN, Cooper DC, Onn SP, Grace AA, Ouimet CC, White FJ, Hyman SE, Surmeier DJ, Girault J, et al. (1998) DARPP-32: regulator of the efficacy of dopaminergic neurotransmission. Science 281:838–842.

Fukuda T, Aika Y, Heizmann CW, Kosaka T (1996) Dense GABAergic input on somata of parvalbumin-immunoreactive GABAergic neurons in the hippocampus of the mouse. Neurosci Res 26:181–194.

Fukuda T, Aika Y, Heizmann CW, Kosaka T (1998) GABAergic axon terminals at perisomatic and dendritic inhibitory sites show different immunoreactivities against two GAD isoforms, GAD67 and GAD65, in the mouse hippocampus: a digitized quantitative analysis. J Comp Neurol 395:177–194.

Gerfen CR (1984) The neostriatal mosaic: compartmentalization of corticostriatal input and striatonigral output systems. Nature 311:461–464.

Gerfen CR, Surmeier DJ (2011) Modulation of striatal projection systems by dopamine. Annu Rev Neurosci 34:441–466.

Gerfen CR, Miyachi S, Paletzki R, Brown P (2002) D1 dopamine receptor supersensitivity in the dopamine-depleted striatum results from a switch in the regulation of ERK1/2/MAP kinase. J Neurosci 22:5042–5054.

Girasole AE, Lum MY, Nathaniel D, Bair-Marshall CJ, Guenthner CJ, Luo L, Kreitzer AC, Nelson AB (2018) A subpopulation of striatal neurons mediates levodopa-induced dyskinesia. Neuron 97:787–795.e6.

Graybiel AM, Ragsdale CW Jr, Yoneoka ES, Elde RP (1981) An immunohistochemical study of enkephalins and other neuropeptides in the striatum of the cat with evidence that the opiate peptides are arranged to form mosaic patterns in register with the striosomal compartments visible by acetylcholinesterase staining. Neuroscience 6:377–397.

Greengard P, Allen PB, Nairn AC (1999) Beyond the dopamine receptor: the DARPP-32/protein phosphatase-1 cascade. Neuron 23:435–447.

Herkenham M, Pert CB (1981) Mosaic distribution of opiate receptors, parafascicular projections and acetylcholinesterase in rat striatum. Nature 291:415–418.

Hersch SM, Ciliax BJ, Gutekunst CA, Rees HD, Heilman CJ, Yung KK, Bolam JP, Ince E, Yi H, Levey AI (1995) Electron microscopic analysis of D1 and D2 dopamine receptor proteins in the dorsal striatum and their synaptic relationships with motor corticostriatal afferents. J Neurosci 15:5222–5237.

Hintiryan H, Foster NN, Bowman I, Bay M, Song MY, Gou L, Yamashita S, Bienkowski MS, Zingg B, Zhu M, Yang XW, Shih JC, Toga AW, Dong HW (2016) The mouse cortico-striatal projectome. Nat Neurosci 19:1100–1114.

Hunnicutt BJ, Jongbloets BC, Birdsong WT, Gertz KJ, Zhong H, Mao T (2016) A comprehensive excitatory input map of the striatum reveals novel functional organization. Elife 5:e19103.

Jones SR, Garris PA, Kilts CD, Wightman RM (1995) Comparison of dopamine uptake in the basolateral amygdaloid nucleus, caudate-putamen, and nucleus accumbens of the rat. J Neurochem 64:2581–2589.

Kuroiwa M, Hamada M, Hieda E, Shuto T, Sotogaku N, Flajolet M, Snyder GL, Hendrick JP, Fienberg A, Nishi A (2012) Muscarinic receptors acting at pre- and post-synaptic sites differentially regulate dopamine/DARPP-32 signaling in striatonigral and striatopallidal neurons. Neuropharmacology 63:1248–1257.

Levey AI, Hersch SM, Rye DB, Sunahara RK, Niznik HB, Kitt CA, Price DL, Maggio R, Brann MR, Ciliax BJ (1993) Localization of D1 and D2 dopamine receptors in brain with subtype-specific antibodies. Proc Natl Acad Sci USA 90:8861–8865.

Lundblad M, Picconi B, Lindgren H, Cenci MA (2004) A model of L-DOPA-induced dyskinesia in 6-hydroxydopamine lesioned mice: relation to motor and cellular parameters of nigrostriatal function. Neurobiol Dis 16:110–123.

Lundblad M, Usiello A, Carta M, Håkansson K, Fisone G, Cenci MA (2005) Pharmacological validation of a mouse model of l-DOPA-induced dyskinesia. Exp Neurol 194:66–75.

Marcott PF, Gong S, Donthamsetti P, Grinnell SG, Nelson MN, Newman AH, Birnbaumer L, Martemyanov KA, Javitch JA, Ford CP (2018) Regional heterogeneity of D2-receptor signaling in the dorsal striatum and nucleus accumbens. Neuron 98:575–587.e4.

Miyamoto Y, Katayama S, Shigematsu N, Nishi A, Fukuda T (2018) Striosome-based map of the mouse striatum that is conformable to both cortical afferent topography and uneven distributions of dopamine D1 and D2 receptor-expressing cells. Brain Struct Funct 223:4275–4291.

Nair AG, Castro LRV, El Khoury M, Gorgievski V, Giros B, Tzavara ET, Hellgren-Kotaleski J, Vincent P (2019) The high efficacy of muscarinic M4 receptor in D1 medium spiny neurons reverses striatal hyperdopaminergia. Neuropharmacology 146:74–83.

Nishi A, Kuroiwa M, Miller DB, O'Callaghan JP, Bateup HS, Shuto T, Sotogaku N, Fukuda T, Heintz N, Greengard P, Snyder GL (2008) Distinct roles of PDE4 and PDE10A in the regulation of cAMP/PKA signaling in the striatum. J Neurosci 28:10460–10471.

Nishi A, Kuroiwa M, Shuto T (2011) Mechanisms for the modulation of dopamine d(1) receptor signaling in striatal neurons. Front Neuroanat 5:43.

Onali P, Olianas MC (2002) Muscarinic M4 receptor inhibition of dopamine D1-like receptor signalling in rat nucleus accumbens. Eur J Pharmacol 448:105–111.

Ouimet CC, Langley-Gullion KC, Greengard P (1998) Quantitative immunocytochemistry of DARPP-32-expressing neurons in the rat caudatoputamen. Brain Res 808:8–12.

Pacelli C, Giguère N, Bourque MJ, Lévesque M, Slack RS, Trudeau LE (2015) Elevated mitochondrial bioenergetics and axonal arborization size are key contributors to the vulnerability of dopamine neurons. Curr Biol 25:2349–2360.

Perez XA, Zhang D, Bordia T, Quik M (2017) Striatal D1 medium spiny neuron activation induces dyskinesias in parkinsonian mice. Mov Disord 32:538–548.

Polito M, Guiot E, Gangarossa G, Longueville S, Doulazmi M, Valjent E, Hervé D, Girault JA, Paupardin-Tritsch D, Castro LRV, Vincent P (2015) Selective effects of PDE10A inhibitors on striatopallidal neurons require phosphatase inhibition by DARPP-32. eNeuro 4:ENEURO.0060-15.2015.

Prager EM, Dorman DB, Hobel ZB, Malgady JM, Blackwell KT, Plotkin JL (2020) Dopamine oppositely modulates state transitions in striosome and matrix direct pathway striatal spiny neurons. Neuron 108:1091–1102.e5.

Ren K, Guo B, Dai C, Yao H, Sun T, Liu X, Bai Z, Wang W, Wu S (2017) Striatal distribution and cytoarchitecture of dopamine receptor subtype 1 and 2: evidence from double-labeling transgenic mice. Front Neural Circuits 11:57.

Ryan MB, Bair-Marshall C, Nelson AB (2018) Aberrant striatal activity in parkinsonism and levodopa-induced dyskinesia. Cell Rep 23:3438–3446.e5.

Salgado S, Kaplitt MG (2015) The nucleus accumbens: a comprehensive review. Stereotact Funct Neurosurg 93:75–93.

Santini E, Valjent E, Usiello A, Carta M, Borgkvist A, Girault JA, Hervé D, Greengard P, Fisone G (2007) Critical involvement of cAMP/DARPP-32 and extracellular signal-regulated protein kinase signaling in L-DOPA-induced dyskinesia. J Neurosci 27:6995–7005.

Schallert T, Tillerson JL (2000) Intervention strategies for degeneration of dopamine neurons in parkinsonism. In: Central nervous system diseases:

innovative animal models from lab to clinic (Emerich DF, Dean RL, Sanberg PR, eds), pp 131–151. Totowa: Humana Press.

Spigolon G, Fisone G (2018) Signal transduction in L-DOPA-induced dyskinesia: from receptor sensitization to abnormal gene expression. J Neural Transm (Vienna) 125:1171–1186.

Svenningsson P, Nishi A, Fisone G, Girault JA, Nairn AC, Greengard P (2004) DARPP-32: an integrator of neurotransmission. Annu Rev Pharmacol Toxicol 44:269–296.

Tanimura A, Du Y, Kondapalli J, Wokosin DL, Surmeier DJ (2019) Cholinergic interneurons amplify thalamostriatal excitation of striatal indirect pathway neurons in Parkinson's disease models. Neuron 101:444–458.e6.

Threlfell S, Sammut S, Menniti FS, Schmidt CJ, West AR (2009) Inhibition of phosphodiesterase 10A increases the responsiveness of striatal projection neurons to cortical stimulation. J Pharmacol Exp Ther 328:785–795.

Voorn P, Vanderschuren LJ, Groenewegen HJ, Robbins TW, Pennartz CM (2004) Putting a spin on the dorsal-ventral divide of the striatum. Trends Neurosci 27:468–474.

Wei W, Ding S, Zhou FM (2017) Dopaminergic treatment weakens medium spiny neuron collateral inhibition in the parkinsonian striatum. J Neurophysiol 117:987–999.

Xenias HS, Ibáñez-Sandoval O, Koós T, Tepper JM (2015) Are striatal tyrosine hydroxylase interneurons dopaminergic? J Neurosci 35:6584–6599.

Yin HH, Knowlton BJ (2006) The role of the basal ganglia in habit formation. Nat Rev Neurosci 7:464–476.

Yung KK, Bolam JP, Smith AD, Hersch SM, Ciliax BJ, Levey AI (1995) Immunocytochemical localization of D1 and D2 dopamine receptors in the basal ganglia of the rat: light and electron microscopy. Neuroscience 65:709–730.